NASA-TM-81366 19820005276

NASA Technical Memorandum 81366

ANALYSIS OF A LONGITUDINAL PILOT-INDUCED OSCILLATION EXPERIENCED ON THE APPROACH AND LANDING TEST OF THE SPACE SHUTTLE

John W. Smith

December 1981

NASA

NASA Technical Memorandum 81366

ANALYSIS OF A LONGITUDINAL PILOT-INDUCED OSCILLATION EXPERIENCED ON THE APPROACH AND LANDING TEST OF THE SPACE SHUTTLE

John W. Smith
Dryden Flight Research Facility
Ames Research Center
Edwards, California

National Aeronautics and
Space Administration
Scientific and Technical
Information Branch

1981

ANALYSIS OF A LONGITUDINAL PILOT-INDUCED OSCILLATION EXPERIENCED ON THE APPROACH AND LANDING TEST OF THE SPACE SHUTTLE

John W. Smith
Dryden Flight Research Facility
Ames Research Center

INTRODUCTION

During the final free flight (FF-5) of the shuttle's approach and landing test (ALT) phase, the vehicle underwent pilot-induced oscillations (PIO's) near touchdown (refs. 1 to 3). The oscillations were present in both the pitch and roll axes and were initiated when the pilot made pitch controller inputs in an effort to control sink rate by changing pitch attitude. Because the control inputs were large and fairly rapid, the elevons rate limited in the pitch axis at the maximum priority rate limit set in the computers. The elevon rate limit also limits the vehicle's roll control capability, and this was partially responsible for the lateral control problem.

Several unpublished studies indicate that time delays as well as priority rate limiting were a significant factor in the PIO's. A simulator study of the effect of time delays on shuttle PIO's is reported in reference 4.

This report describes the combined effect of pilot input rate limiting and time delays. Frequency responses are predicted for various parameters under rate saturated conditions by using nonlinear analysis.

SYMBOLS AND ABBREVIATIONS

Physical quantities in this report are given in the International System of Units (SI) and parenthetically in U.S. Customary Units. The measurements were taken in U.S. Customary Units. Factors relating the two systems are presented in reference 5.

A/C	aircraft
ALT	approach and landing test
APU	auxiliary power unit
a_n	normal acceleration, g
C_D	drag coefficient, $\frac{\text{Drag}}{\bar{q}S}$
C_{D_α}	change in drag coefficient with angle of attack, $\frac{\partial C_D}{\partial \alpha}$, per rad
$C_{D_{\delta_e}}$	change in drag coefficient with elevator deflection, $\frac{\partial C_D}{\partial \delta_e}$, per rad
C_L	lift coefficient, $\frac{\text{Lift}}{\bar{q}S}$
C_{L_α}	lift-curve slope, $\frac{\partial C_L}{\partial \alpha}$, per rad
$C_{L_{\delta_e}}$	change in lift coefficient with elevator deflection, $\frac{\partial C_L}{\partial \delta_e}$, per rad
C_m	pitching moment coefficient, $\frac{\text{Pitching moment}}{\bar{q}S\bar{c}}$
C_{m_q}	pitch damping derivative, $\frac{\partial C_m}{\partial q \frac{\bar{c}}{2V}}$, per rad
C_{m_α}	static longitudinal stability derivative, $\frac{\partial C_m}{\partial \alpha}$, per rad
$C_{m_{\delta_e}}$	change in pitching moment coefficient with elevator deflection, $\frac{\partial C_m}{\partial \delta_e}$, per rad
$\bar{c}$	mean aerodynamic chord, m (ft)
c_{ref}	overall vehicle length, m (ft)
cg	center of gravity
FF	free flight
f( )	function of parameter inside the parentheses

h_p	altitude, m (ft)
I_y	moment of inertia about y-axis, N-m^2 (slug-ft^2)
$j\omega$	imaginary part of root, per sec
K	gain constant
K_s	gain factor out of the shaping function
M	Mach number
PIO	pilot-induced oscillation
q	pitch rate, rad/sec
$\bar{q}$	dynamic pressure, N/m^2 (lb/ft^2)
S	reference area, m^2 (ft^2)
s	Laplace transform variable, per sec
T	time delay, sec
Ts	transfer function
t	time, sec
u, V	velocity, m/sec (ft/sec)
w	weight, kg (lb)
α	angle of attack, deg
Δ	transfer function denominator
δ_e	elevon deflection, deg or rad
δ_{e_c}	commanded input, rad
δ_{e_p}	pilot input, deg or rad
δ_{e_s}	shaping function output, deg or rad
θ_0	trim attitude, deg or rad

θ	pitch attitude, deg or rad
τ	time constant, sec
φ	phase angle, deg
ω	frequency, rad/sec

Subscripts:

CP	cockpit
c	commanded
e	error signal
p	pilot
R	generalized input
ref	reference
1, 2, 3, . . .	sequential calculation

A dot over a quantity denotes the first derivative with respect to time.

VEHICLE DESCRIPTION

Aircraft and Test Configuration

The space shuttle vehicles were built by Rockwell International under a contract awarded by the National Aeronautics and Space Administration. The first vehicle, which was designed for unpowered flight, was to be flown in approach and landing tests only.

The shuttle used for the approach and landing tests was carried aloft on the fuselage of a modified B-747 airplane and then launched at an altitude and position within gliding distance of a dry lakebed at Edwards Air Force Base. Five glide flights were made with this vehicle. A special tail cone was installed to cover and streamline the aft portion of the vehicle. The first three flights were flown with the tail cone installed. On the last two flights, the tail cone was removed and dummy engines were installed to simulate the drag or aft profile that would exist on the rocket-launched shuttle during the orbital flight tests.

The ALT configuration has essentially the same flight characteristics as the orbital flight test configuration. There are slight differences in the aircraft dynamics due to the differences in weight and inertia and the thermal protection system on the reentry vehicle. This study is limited to the ALT vehicle.

Figure 1 is a three-view drawing illustrating the relative size and location of the primary control surfaces of the shuttle. Pertinent physical characteristics are presented in table 1.

Primary Flight Control Systems

Aerodynamic surfaces.— Full span independently actuated elevons provide both pitch and roll control. A conventional rudder mounted on the trailing edge of a single vertical stabilizer provides directional control. Speed brakes are activated by mechanically splitting the rudder symmetrically. A flap on the lower aft fuselage provides active trim control.

Control systems.— A digital fly-by-wire control system is implemented on the space shuttle. All elements of the control system, including the hand controller electrical signals, sensors, computers, and electrical paths up to the servoactuators, are quadruply redundant. Three independent hydraulic systems (APU's) supply power to the surface actuators. The independent operation of the four control systems and three hydraulic systems provides fail-operational/fail-safe capability.

Rotational hand controller.— Both the commander's and the pilot's station are provided with identical rotational hand controllers. In pitch, the controller pivots about the palm of the hand; in roll, it pivots about a point slightly below the base. Therefore, the pilot effectively applies a torque gradient rather than a force gradient. The commander's and the pilot's station controllers are not mechanically linked, but if both are deflected the input signals are combined and the elevons are deflected accordingly. However, the controllers are spring centered and null at zero electrical output.

Pilot control and augmentation.— A pitch rate command system is used on the space shuttle for the approach and landing phases of flight. The system is implemented as a digital flight control system resident in the onboard flight control computers. The mathematical block diagram in figure 2 shows the major elements of the closed-loop pitch attitude control system. The rotational hand controller input, δ_{e_p}, commands an output given by the pitch stick shaping function. The shaping function output, δ_{e_s}, is prefiltered to form the pitch rate command, $\dot{\theta}_c$. In the forward path and downstream of the error signal, a lead-lag filter along with a gain term, $f(\bar{q})$, gives the desired pitch rate response. The gain is scheduled as a function of dynamic pressure ($200/\bar{q} = 1.64$ for touchdown). Pitch rate command is achieved by positive feedback around the power actuator and servo, yielding an equivalent system for the actuator loop with a "free" s in the denominator. As such, the error signal, which is made up of the commanded response and aircraft pitch rate, is continually driven to zero. Therefore, the integration rate is proportional to the scheduled gain. Internal to the actuator and servo loop, the priority rate at which the actuator can move is restricted to 20 degrees per second, and the travel limit, which has been changed, is restricted for the following calculations to 21.5°. The filters, gains, summations, restrictions, and pitch stick shaping function are implemented in the shuttle's digital flight control computers.

A more complete description of the total flight control system and its design is given in reference 6.

ANALYSIS AND DISCUSSION

Shuttle PIO Experience

The first four landings of the ALT shuttle configuration were made on the lakebed without incident, as reported in references 2 and 3. The handling qualities were judged to be good; longitudinal control was rated approximately 2 on the Cooper-Harper scale (ref. 3).

A precision landing on the runway was attempted during the last flight. During the landing, the pilot induced both a longitudinal and a lateral PIO. The PIO first occurred in the pitch axis and then propagated to the roll axis. The oscillation was initiated by pitch controller inputs that were made to control sink rate. The excessive controller inputs caused the elevons to rate saturate. A right roll disturbance was then introduced as the main gear touched the runway. A lateral PIO then followed because roll control was restricted by priority rate limiting and control authority, which favored the pitch axis. The combined time of the oscillations was more than 12 seconds, and both oscillations were near the same frequency. Because the oscillations originated in pitch, it was assumed that the PIO problem was primarily a longitudinal control problem, with the roll control problem system induced. The flight conditions near the time of the PIO's are listed in table 2.

Figure 3 presents a time history illustrating the longitudinal PIO. Pilot inputs to the hand controller, δ_{e_p}, were approximately 0.5 hertz and in excess of 20° peak to peak. The average travel of the elevons was about 15° peak to peak. In addition, the control surface time history indicates that the actuators had reached the priority rate limits. The resulting pitch rate during the longitudinal PIO reached a peak to peak value of 7 degrees per second and appeared to be neutrally stable.

Prior investigations had predicted the shuttle to be susceptible to PIO's. An analytical study based on the shuttle's aerodynamics concluded that the shuttle would be prone to a longitudinal PIO (ref. 1). Also, simulator studies conducted concurrently with the approach and landing tests, as reported in reference 2, showed a tendency towards PIO's.

After the PIO's were experienced during FF-5, the rotational hand controller signal shaping was modified to include a suppression filter like that reported in references 7 and 8, and an analytical study was undertaken to investigate and evaluate the following:

1. System lag caused by rate limiting in the actuator loop.

2. The effect of varying the rotational hand controller input on the total attenuation and phase lag.

3. The effect of time delay in the augmentation loop on the gain and phase lag.

The following section gives an analytical description of the longitudinal or pitch control mode implemented on the shuttle.

Pitch Control Modeling

Presented in figure 4 is a conceptual block diagram of the shuttle control system. The pilot attempts to minimize pitch attitude error; he also tries to maintain the desired sink rate by changing the vehicle's reference attitude. The amount of rotation or torque applied by the pilot to the controller per unit error signal is referred to as pilot gain.

Figure 5 shows the parabolic hand controller shaping function programmed on the shuttle. The primary purpose of the shaping function, as it is in most fly-by-wire systems, is to increase the gain as a nonlinear function of controller displacement. Figure 6 presents the gain variation as a function of controller input, δ_{e_p}. In the command path and downstream of the shaping function, a gain constant of 0.4 degrees per second per degree is scheduled for the final approach and landing phases of flight. The pitch rate commanded, therefore, is $\delta_{e_p} \frac{\Delta\delta_{e_s}}{\Delta\delta_{e_p}} 0.4$. To improve the handling qualities, a lead-lag filter, $1.5 \frac{(s + 1.8)}{(s + 2.7)}$, is cascaded in the forward path of the augmentation loop.

It was reasoned that dead time resulting from transport lag plus the delay due to the rather low rotational hand controller sample rate of 12.5 cycles per second had worsened the PIO problem. Consequently, in the analysis a time delay function e^{-Ts} was added into the forward path of the augmentation loop. To assess the effect of this type of nonlinearity on the closed- and open-loop behavior of the system, the time delay function, T, was assigned various values: 0, 0.1, 0.2, and 0.4 second. Pitch rate command was achieved by positive feedback around the power actuator and servomechanism, as shown in figure 7. The system for the actuator loop with no rate limiting is given by

$$\frac{\delta_e}{\delta_{e_c}} = \frac{(s/1.5 + 1)}{s(s/30 + 1)}$$

Therefore, the integration rate was proportional to the gain $f(\bar{q})$ (fig. 4), where $f(\bar{q}) = \frac{200}{\bar{q}} = 1.64$.

During FF-5, the longitudinal control system underwent an extensive amount of rate limiting prior to touchdown, as is evident in the elevator time history of figure 3. The boundary limits of both position and rate limit as a function of input amplitude and frequency are presented in figure 8. Three δ_{e_p} inputs are shown parametrically as

a function of frequency. These variations were obtained from a linear calculation with the shaping gain equivalent to the peak controller input. At realistic trim conditions and from controller inputs, δ_{e_p}, up to 15°, the system would only experience priority rate limiting over the frequency range shown. For controller inputs typical of the PIO condition of FF-5 ($\delta_{e_p} = 10°$), the system would rate limit at 2.5 to 3.0 radians per second. Because rate limiting would be expected to add phase lag into the overall system, the actuator loop was first investigated in a separate or isolated fashion.

Presented in figure 9 is a time history typical of the digital simulation of just the actuator loop. For this particular example, the input amplitude to the actuator was 10° at a frequency of 3 radians per second. The system rate limited at 20 degrees per second over 90 percent of the time, and the through gain based on peak values was less than unity. Several computations were made at various frequencies and amplitudes to obtain a broad comparison to a model of the actuator loop.

Figure 10 compares both the amplitude ratio and the phase angle of the digital simulation to the algorithm that describes the actuator model. For a value of δ_{e_c} of 10° (near the PIO condition), the rate limit causes attenuation from 3 radians per second on. Additional phase lag is also added into the system from there on. The algorithm describing the actuator model is developed and presented as a subroutine in appendix A.

Integrated Analysis of the PIO

Nonlinear method.— During the PIO, an extensive amount of rate saturation prevailed. In addition, it was estimated (as reported in ref. 2) that up to 0.38 second of equivalent time delay may have been present in the augmentation loop (fig. 4). Therefore, a realistic analysis requires consideration of these two nonlinearities as well as the gain variation through the shaping function. The following discussion utilizes a nonlinear computation of the system gain and phase as a function of pilot input and frequency.

The method, in general, is simply to assign a value to the error vector, which has amplitude and frequency but phase equal to zero. Then an input/output vector can be computed successively through each element, keeping track of amplitude and phase algebraically until an open-loop vector for the augmentation loop is obtained. The input to the augmentation loop is then determined by adding the feedback vector to the error vector. The reciprocal or inverse functions in the command path (reversing the direction of flow) are used to obtain the pilot input, δ_{e_p}. This then gives a closed-loop vector relationship of the desired elements as a function of δ_{e_p} and frequency.

Appendix B outlines the nonlinear computational procedure. The aircraft aerodynamics and transfer functions are presented in table 3.

Elevon attenuation and system response characteristics.— If the amplitude of the input is great enough, elevon travel will be attenuated due to rate limiting as frequency is increased. Figure 11 presents the elevon travel as a function of controller input, δ_{e_p}, and frequency. Also shown are the boundary curves for minimum perceptible and fully developed rate limiting. For inputs of 5°, no attenuation is expected because of rate limiting for frequencies up to 8 radians per second, as indicated by the circle symbols, which remain below the minimum rate limit boundary. At δ_{e_p} = 10° the elevons are fully limited in a sawtooth fashion at frequencies from 3.5 radians per second on. If the input increases to 15°, the rate limiting begins at approximately 2 radians per second and then follows the fully developed rate limit boundary identical to the 10° input.

The effect of time delay on elevon amplitude as a function of frequency is shown in figure 12. Time delay is varied parametrically from 0 to 0.4 second. A constant controller input amplitude of 10° is applied to the shaping function. Increasing the time delay increases the elevon amplitude as frequency increases. From 4 radians on, rate limit tends to limit the elevon amplitude, regardless of the amount of dead time.

The normal force response of the aircraft, particularly the crossover phase frequency, is believed to affect pilot ratings. An assessment of the PIO tendencies based on both pitch attitude and the aircraft's normal force response is reported in reference 1. Presented in figure 13 is the effect of time delay on the frequency response of a_n at the cockpit per controller input. A value of 5° was used for the controller input in order to stay below any rate limiting over the frequency range shown. It is clearly evident by the increase in gain and phase lag that an excessive amount of dead time (T = 0.4 sec) causes the aircraft to be more responsive per controller input. The peak increase occurs at frequencies from 2.5 to 3.0 radians per second. For a time delay of 0.4 second the crossover phase frequency (fig. 13(b)) is about 2 radians per second; with no time delay, the crossover phase frequency is above 10 radians per second. The same parameters are shown in figure 14 for three controller inputs at a constant value of dead time, T, of 0.1 second. For a controller input of 5°, the system behaves in a linear fashion. At 10°, the response is attenuated by rate limiting from approximately 2.5 radians per second on. As shown in figure 14(b), rate limiting also adds phase lag into the system.

The calculated frequency response of the shuttle's pitch rate command system is presented in figure 15. A constant value of δ_{e_p} of 5° is applied to the shaping function. The effect of dead time is shown parametrically and is varied from 0 to 0.4 second. Again, and consistent with normal force response characteristics, the system would be highly susceptible to oscillations at approximately 3 radians per second with 0.4 second of dead time in the augmentation. Figure 16 shows the frequency response of the pitch rate command system for a constant value of dead time of 0.1 second at three values of pilot input. For a value of δ_{e_p} of 5°, the system retains linear behavior throughout the frequency range shown. For values of δ_{e_p} of 10° and 15°, rate saturation limits the attenuation, as shown by the diagonal lines. The breakpoint for a value of δ_{e_p} of 10° is approximately 3.5 radians per

second; it is approximately 2 radians per second for $\delta_{e_p} = 15°$. Rate saturation adds about 50° of lag into the system, as shown in figure 16(b).

Figure 17 presents the computed results of pitch attitude response per pilot input versus frequency. Three values of controller input are presented. As pointed out previously, the system behaves in a linear fashion for $\delta_{e_p} = 5°$. The amplitude rates normally decrease at 20 decibels per decade until the system starts to rate limit. The breakpoint occurs at 2.0 and 3.5 radians per second for values of δ_{e_p} of 15° and 10°, respectively. The crossover phase frequency is approximately 3.5 radians per second for both 5° and 10° of δ_{e_p} (fig. 17(b)). About 70° of additional phase lag is added into the attitude system at maximum pilot inputs.

In order to sustain an oscillation in a closed-loop system, the total gain must be unity at a phase shift of -180° (Nyquist criteria). Assuming that the pilot acts as pure gain and with no phase changes, the pilot gain required to cause a PIO would be the gain margin at a -180° phase shift. Because of system nonlinearities, the critical pilot gain is also a function of controller input, δ_{e_p}. Figure 18 presents PIO frequency and critical pilot gain variation as a function of pilot input for various values of dead time. Increasing the pilot input decreases the pilot gain required to PIO. This effect is due primarily to the increase in gain across the shaping function with an increase in δ_{e_p} (fig. 6). Increasing the amount of dead time in the augmentation loop reduces both the crossover frequency and pilot gain required to PIO. For reasonable values of dead time (T = 0.1 sec), the critical pilot gain would be reduced at least 50 percent.

CONCLUSIONS

A longitudinal PIO experienced on the shuttle was analyzed by a nonlinear technique. In general, the analysis indicates that:

1. For controller inputs of 5° or less with no dead time, the control system behaves in a linear fashion.

2. For 10° of controller inputs, regardless of the amount of dead time, the elevon loop rate saturates at frequencies above 4 radians per second.

3. The pitch attitude crossover phase frequency is about 3.5 radians per second for both the 5° and 10° controller input.

4. At the PIO condition, rate limiting in the forward path decreases the system gain and also adds phase lag into the system.

5. Increasing the amount of dead time reduces the phase crossover frequency and reduces the pilot gain required to PIO. An excessive amount of dead time (0.4 second, for example) significantly increases the PIO tendencies.

APPENDIX A— MATHEMATICAL DESCRIPTION OF THE ACTUATOR LOOP

A pitch rate command system was used on the shuttle for the approach and landing phases of flight. The system was designed such that the error signal in the augmentation loop was continuously driven to zero so that the output or vehicle pitch rate actively tried to match the commanded input (type 1 system). To effect the necessary integration, positive feedback was implemented around just the actuator loop, as shown in figure 19. To provide lead in the system, a first order lag was programmed in the actuator loop feedback path. Also, the preselected or priority rate limit plus the travel limitations were programmed in the forward path of the actuator loop. However, for this particular investigation, travel restriction was not necessary; consequently, for this study that gain factor was always unity. Because of the nonlinear nature that existed in just this part of the system, it was felt worthwhile and convenient to define and investigate the actuator loop separately.

In general, what was desired was an input/output relationship that was a function of the same input. In the development of the nonlinear algorithm, it was found expedient and useful to begin with a linear input/output relationship. This was accomplished by iterating around the loop with both nonlinear elements, G6 and G7, equal to unity. With reference to the following subroutine, consider first the input signal XX (line 7), which is a vector having amplitude, phase, and frequency.

```
      SUBROUTINE TING(XX,Z)
      COMMON /TFS/S
      COMMON /JAKE/X(5),ZX,YNEW,Y,W,A,PHI,XX2
      COMPLEX S,XX,Y,Z,W,X,YNEW,G6,G7
 5    COMPLEX ZX,XX2
      N=100
      Y=XX
      DO 10 K=1,N
      X(1)=Y+XX
10    X(2)= S*X(1)
      X(3)=X(2)
      X(4)= (1/S)*X(3)
      X(5)= X(4)
      Z= (20/(S+20))*X(5)
15    YNEW=(1.5000/(S+1.50000))*Z
      IF(ABS(CABS(Y)-CABS(YNEW)).LE.0.00001) GO TO 11
      Y    = YNEW
   10 CONTINUE
   11 CONTINUE
20    X(2)= S*X(1)
      X(3)=G6(X(2))
      X(4)= (1/S)*X(3)
      A=CABS(X(4))
      SIG =REAL(X(4))
25    OMG =AIMAG(X(4))
      PHI = 1.570796
      IF(SIG.EQ.0.0) GO TO 6
      PHI =ATAN2(OMG,SIG)
    6 CONTINUE
30    DEL = 0.0
      IF(CABS(X(1))*AIMAG(S).LE..548) GO TO 7
      VV = .548/(CABS(X(1))*AIMAG(S))
      DEL = 1.570796*VV -1.570796
    7 CONTINUE
35    TPD =PHI + DEL
      U = A* SIN(TPD)
      V = A*COS(TPD)
      X(4)= CMPLX (V,U)
      X(5)= X(4)
40    Z= (20/(S+20))*X(5)
      Y    =(1.5000/(S+1.50000))*Z
      W = Z/(X(1)-Y)
      Z =W*XX
      A=CABS(W)
45    SIG=REAL(W)
      OMG=AIMAG(W)
      PHI=90
      IF(SIG.EQ.0.0) GO TO 12
      PHI= ATAN2(OMG,SIG)*57.296
50    12 CONTINUE
      ZX=Z
      XX2=XX
      RETURN
      END
```

Next, sum the input signal with Y and initialize for the first iteration by setting Y equal to XX. The vector X(1) will then be differentiated to obtain the rate vector necessary for subsequent computations. Throughout the first series of iterations the rate restriction G6 is equal to unity gain, or X(3) = X(2). The vector X(3) is integrated to get back to a position vector X(4). Since there is no appreciable amount of travel limitation, the vector X(5) will equal the vector X(4), or the gain of G7 will be unity. A first-order lag was used to approximate the power actuator characteristics. That is,

$$Z = \frac{20}{(s + 20)} X(5)$$

and

$$YNEW = \frac{5}{(s + 1.5)} Z$$

A test follows at this point to determine whether the desired convergence (1×10^{-5}) has been obtained. If not, Y is replaced by YNEW and the procedure is repeated until the desired convergence is reached. When the "if statement" is satisfied, the computation continues or leads into the nonlinear computation (FORTRAN statement 11 on). The final value of the vector X(1) from the previous iteration is differentiated to get X(2). The rate restriction is then applied to X(2). In other words, X(3) = G6 (X(2)).

However, the maximum gain for the sawtooth type of wave form rate limiting is used for these computations, as follows:

$X(3) \leqslant (20/57.3)\pi/2 = 0.548$ rad/sec

The rate limit (0.548) is entered into the following function subprogram.

```
      COMPLEX FUNCTION G6(X)
      COMPLEX X,CLIM
      COMPLEX A
      A=X
      A=CLIM(A,.548)
      G6=A
      RETURN
      END
```

A general limiting algorithm is represented by another function subprogram.

```
      COMPLEX FUNCTION CLIM(A,X)
      COMPLEX A,B
      Y=CABS(A)
      IF(Y.EQ.0.0) GO TO 1
      B=A
      IF(Y.GT.X) B=(X/Y)*A
      CLIM=B
      RETURN
    1 CONTINUE
      CLIM=CMPLX(X,0.0)
      RETURN
      END
```

Integrating X(3) gives a new position vector X(4). Next, the absolute value, real, and imaginary parts plus the phase angle of X(4) are determined. From FORTRAN statement 6 on down to statement 7, a new phase angle is computed based on the intersection of a sinusoidal oscillation and a rate limited wave train oscillation. This new angle (TPD) is then used to compute a new vector for the forward path. A final computation gives the vector amplitude ratio, W, representing the nonlinear system as a function of the initial input vector, XX.

APPENDIX B— BASIC NONLINEAR ANALYSIS AND COMPUTATIONAL PROCEDURE

The flow diagram shown in figure 20 represents the shuttle's basic control system, aerodynamics, and normal acceleration at the cockpit.

In the diagram, T1 represents the pilot transfer function, and for this study T1 will be considered a pure gain term. T2 is the nonlinear shaping function shown in figure 5. All transfer functions or the inverse functions of T1, T2, T3, and T4 are presented in tables 3 and 4, except for the actuator algorithm T7, and that function is derived and presented as a subroutine in appendix A.

To obtain an open-loop frequency response for the pilot loop, an absolute value is assigned to X1, which will be the pilot input to the shaping function for unity pilot gain. The task in general is to find an absolute value for X2 that is close to X1. For example; let δ_{e_p} equal 5° of pilot input, or X1 equal 0.0873 radian. The desired accuracy is ABS(CABS(X1) - CABS(X2) $\leqslant 1 \times 10^{-5}$.

The first iteration is initiated through a "do loop" by assigning a number to the real part of X7, such as

I = 1, 1000

SIG Z7 = 1.0 X I

Next, the vector signal is traced around through each block, including the inverse functions to the left of the augmentation summation junction.

Now, if and when CABS X2 > X1, the previous computation for I is used. So RBASE = I - 1 or a new index is J = 1, 10 and SIG X7 = RBASE + J(0.1).

The above scheme is repeated six times, moving to the left one decimal point at a time and proceeding with a new "do loop" until the desired accuracy is obtained. The complex value of each vector is successively computed through each block and summation junction. A final computation then yields the input/output amplitude and phase relationship as a function of pilot input and frequency.

The logic, vector arithmetic, and transfer functions shown in the tables and appendix A for various configurations were programmed on a digital computer. In the equations, s = jω, where ω is a discrete frequency.

Dryden Flight Research Facility
Ames Research Center
National Aeronautics and Space Administration
Edwards, Calif., July 29, 1981

REFERENCES

1. Smith, Ralph H.: Evaluation of Space Shuttle Orbiter Longitudinal Handling Qualities in Approach and Landing. Systems Research Lab., Inc. (2800 Indian Ripple Rd., Dayton, OH 45440), Aug. 1979.

2. Hoey, Robert G., et al.: AFFTC Evaluation of the Space Shuttle Orbiter and Carrier Aircraft - NASA Approach and Landing Test. AFFTC-TR-78-14, Air Force Flight Test Center, Edwards AFB, May 1978.

3. Space Shuttle Orbiter Approach and Landing Test. JSC-13864, NASA Johnson Space Center, Feb. 1978.

4. Riley, Donald R.; and Miller, G. Kimball, Jr.: Simulator Study of the Effect of Control-System Time Delays on the Occurrence of Pilot-Induced Oscillations and on Pilot Tracking Performance With a Space-Shuttle-Orbiter Configuration. NASA TP-1588, 1980.

5. Mechtly, E. A.: The International System of Units—Physical Constants and Conversion Factors. Second Revision. NASA SP-7012, 1973.

6. Space Shuttle Orbital Flight Test: Level C: Functional Subsystem Software Requirements. SD 76-SH-0007B, Rockwell Internat., Space Systems Group, May 1979.

7. Smith, John W.; and Edwards, John W.: Design of a Nonlinear Adaptive Filter for Suppression of Shuttle Pilot-Induced Oscillation Tendencies. NASA TM-81349, 1980.

8. Powers, Bruce G.: Experience With an Adaptive Stick-Gain Algorithm To Reduce Pilot-Induced-Oscillation Tendencies. AIAA Paper No. 80-1571, Aug. 1980.

TABLE 1.—PHYSICAL CHARACTERISTICS

s, m^2 (ft^2)	249.91 (2690)
$\bar{c}$, m (ft)	12.06 (39.56)
c_{ref}, m (ft)	32.77 (107.5)
w, kg (lb)	68,038.50 (150,000)
cg, percent of c_{ref}	66.25
I_y, kg-m^2 (slug-ft^2)	6,833,703.42 (5,040,282)

TABLE 2.—FLIGHT CONDITIONS NEAR TIME OF PILOT-INDUCED OSCILLATIONS

α, deg	7
M	0.32
h_p, m (ft)	≤694.94 (≤2280)
$\bar{q}$, N/m^2 (lb/ft^2)	6654 to 5841 (139 to 122)
V, m/sec (ft/sec)	97.54 (320)
θ_0, deg	7

TABLE 3.—AERODYNAMIC STABILITY COEFFICIENTS AND TRANSFER FUNCTIONS

Body axis stability coefficients:

$C_{D_\alpha} = 0.0053$	$C_{m_q} = -2.00$
$C_{D_{\delta_e}} = 0.0016$	$C_{m_\alpha} = 0.001$
$C_{L_\alpha} = 0.048$	$C_{m_{\delta_e}} = -0.0088$
$C_{L_{\delta_e}} = 0.018$	

Transfer functions:

$$\frac{u}{\delta_e} = \frac{2.44\,(s + 18.48)\,(s + 0.436 \pm j\,0.649)^2}{\Delta}$$

$$\frac{\alpha}{\delta_e} = \frac{-0.226\,(s + 5.99)\,(s + 0.0108 \pm j\,0.0770)^2}{\Delta}$$

$$\frac{q}{\delta_e} = \frac{-1.30\,s(s + 0.648)\,(s + 0.0349)}{\Delta}$$

$$\frac{a_n}{\delta_e} = \frac{2.26\,(s + 2.089)\,(s - 1.754)\,(s + 0.0277)\,(s - 0.0156)}{\Delta}$$

where

$$\Delta = (s + 0.0945 \pm j\,0.122)^2\,(s + 0.887)\,(s - 0.100)$$

TABLE 4.—TRANSFER FUNCTION DEFINITIONS

[|X1| designated input; $(|X1| - |X2|) \leq K$;
see table 3 for aerodynamic transfer functions]

Function	Vector output
------	X1 = X2 (open loop)
T1 (inverse; pilot transfer function)	$X2 = \frac{1}{\tau + 1} e^{T*s} * X3$, $\tau = 0$, $T = 0$
T2 (inverse hand controller)	$A = \|X4\|$ $B = (13.83 + 20.66 * 57.3 * A)^{0.5}$ $C = -2.569 + B$ $X3 = (C/A * 57.2) * X4$
T3 (inverse)	$X4 = \frac{s + 50}{0.05} * X5$
T4 (inverse)	$X5 = \frac{s + 2.7}{s + 1.8} * 0.667 * X6$
T5	$X8 = 1.64 * X7$
T6	$X9 = e^{-T*s} * X8$, $T = 0.1, 0.2, 0.4$
T7	Subroutine TING (XX, Z) (app. A)
T8	$X11 = 1.0 * X10$ If $\|X11\| > 0.375$, $X11 = \frac{0.375}{\|X11\|} * X11$
T9	$X12 = \frac{\alpha}{\delta_e} * X11$
T10	$X13 = \frac{a_n}{\delta_e} * X11$
T11	$X14 = \frac{u}{\delta_e} * X11$
T12	$X15 = \frac{\dot{\theta}}{\delta_e} * X11$
T13	$X18 = \frac{50}{s + 50} * X15$
T14	$X19 = 1.5 * \frac{s + 1.8}{s + 2.7}$
T15	$X20 = \frac{1}{s} * X15$
T16	$X16 = (1.55 * s) * X15$
T17	$X17 = 1.0 * X13$ $X6 = X19 - X7$ $X21 = X16 + X17$ } Summations

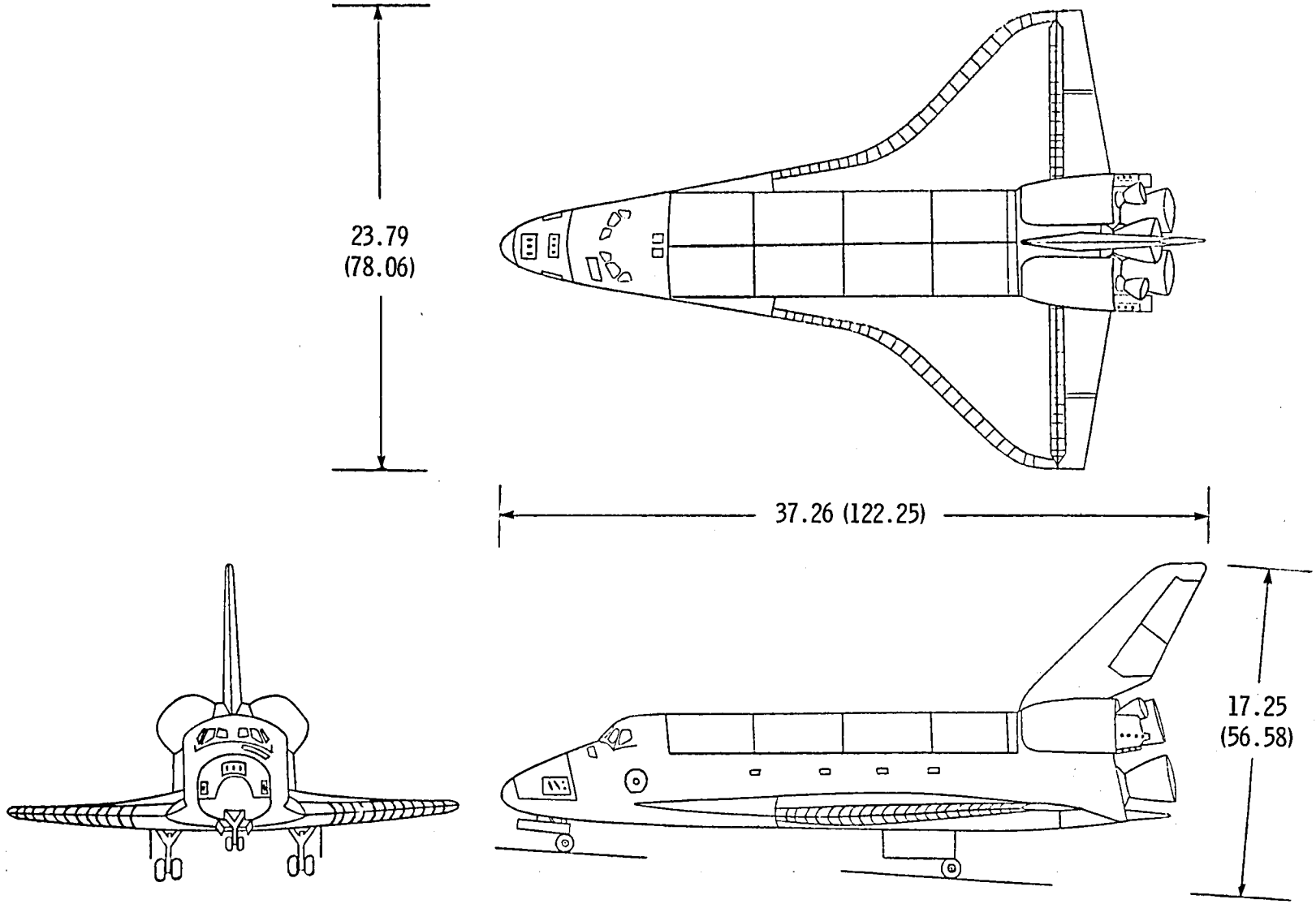

Figure 1. Three-view drawing of shuttle. Dimensions in meters (feet).

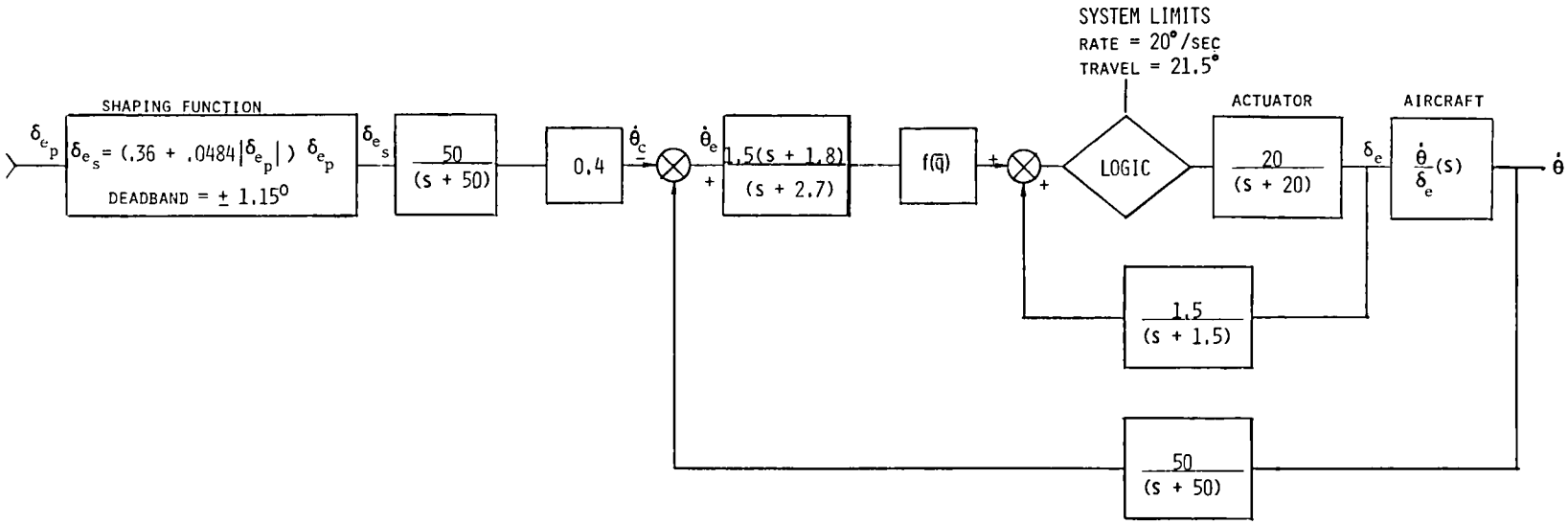

Figure 2. Mathematical description of shuttle pitch attitude control system.

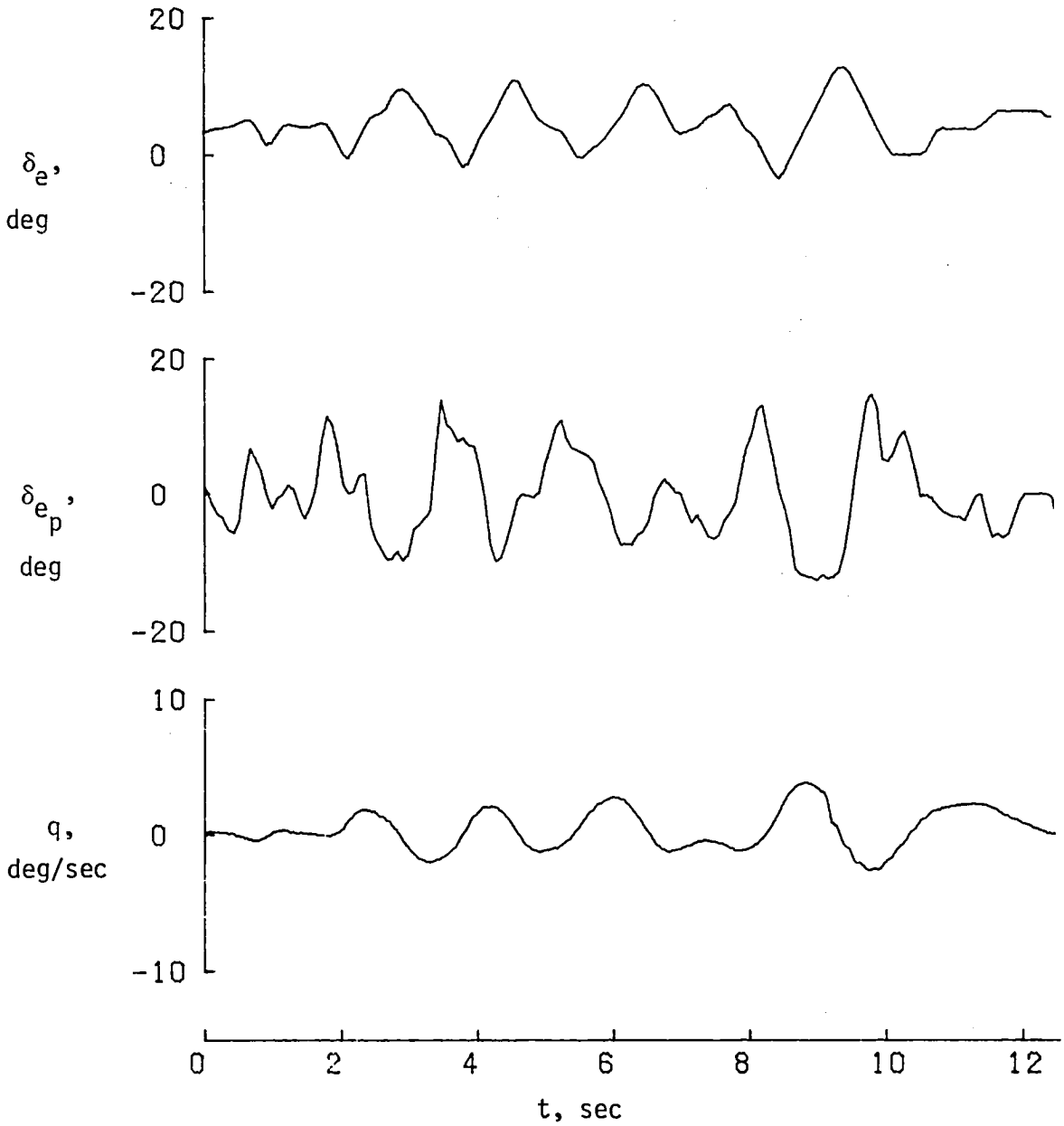

Figure 3. Time history of pilot-induced oscillation undergone by shuttle during approach and landing test FF-5.

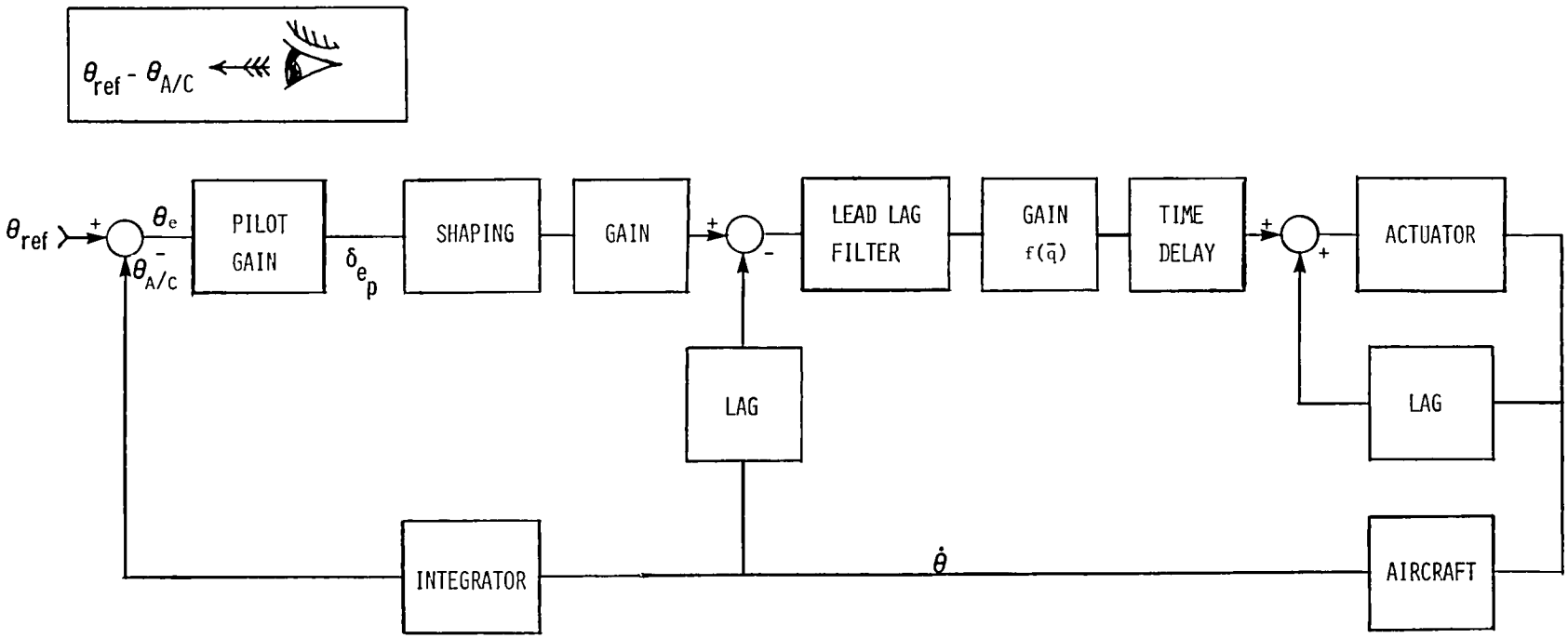

Figure 4. Conceptual block diagram of shuttle control system with pilot closing the pitch attitude loop.

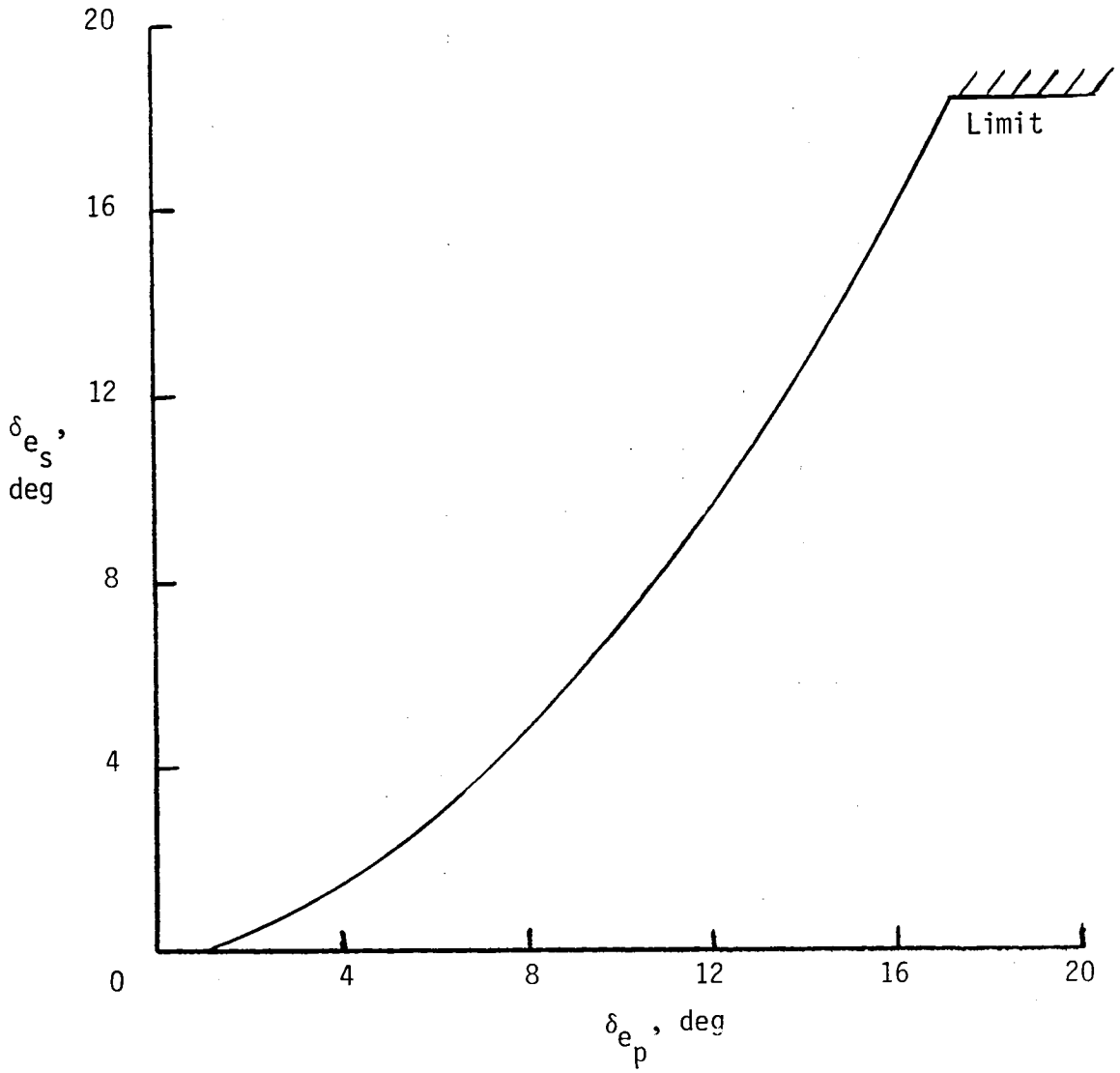

Figure 5. Shuttle longitudinal rotational hand controller shaping function. $\delta_{e_s} = \left(0.36 + 0.0484 \left|\delta_{e_p}\right|\right) \delta_{e_p}$; deadband = ±1.15.

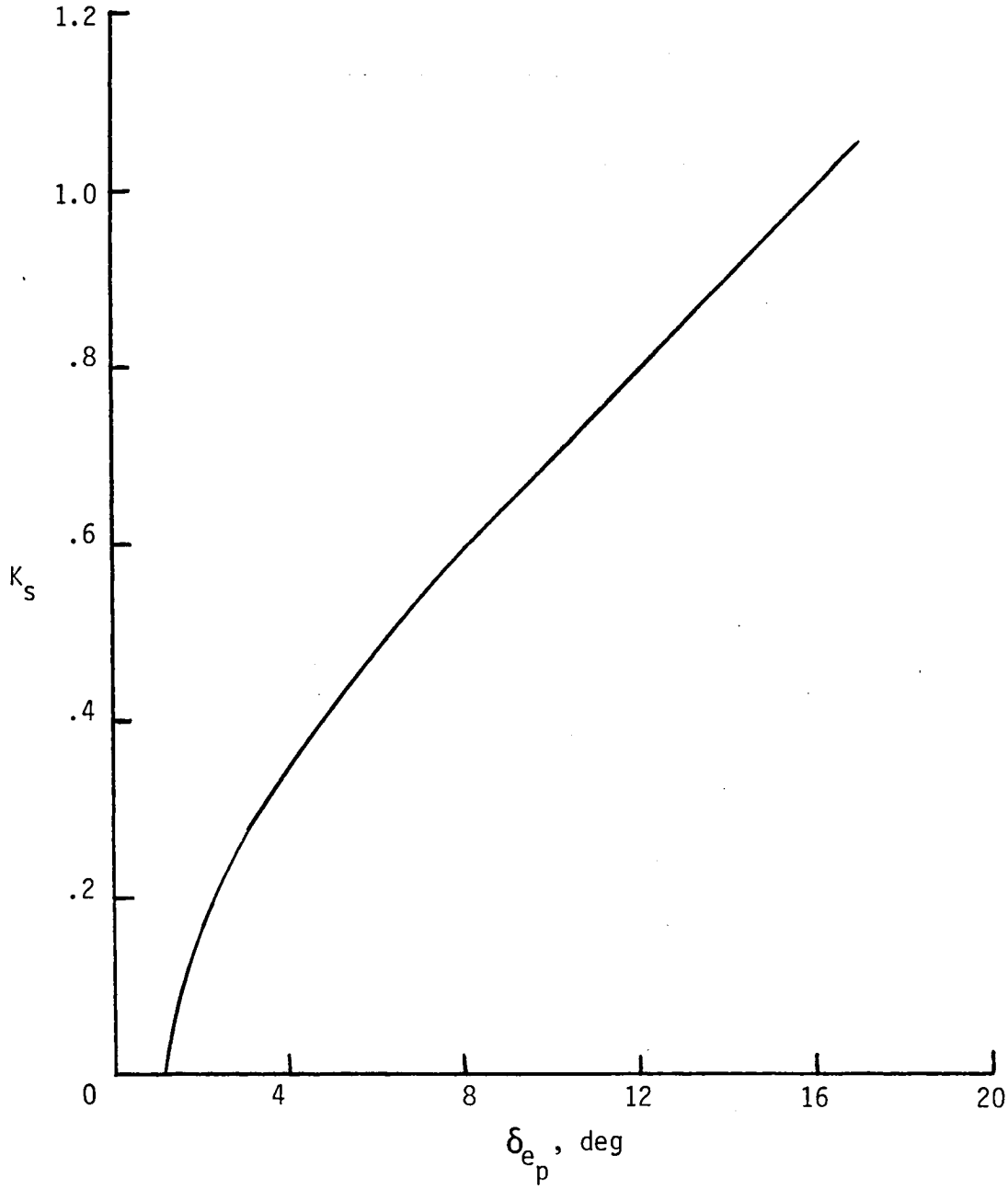

Figure 6. Shuttle longitudinal rotational hand controller shaping function gain. $K_s = \frac{\Delta\delta_{e_s}}{\Delta\delta_{e_p}}$

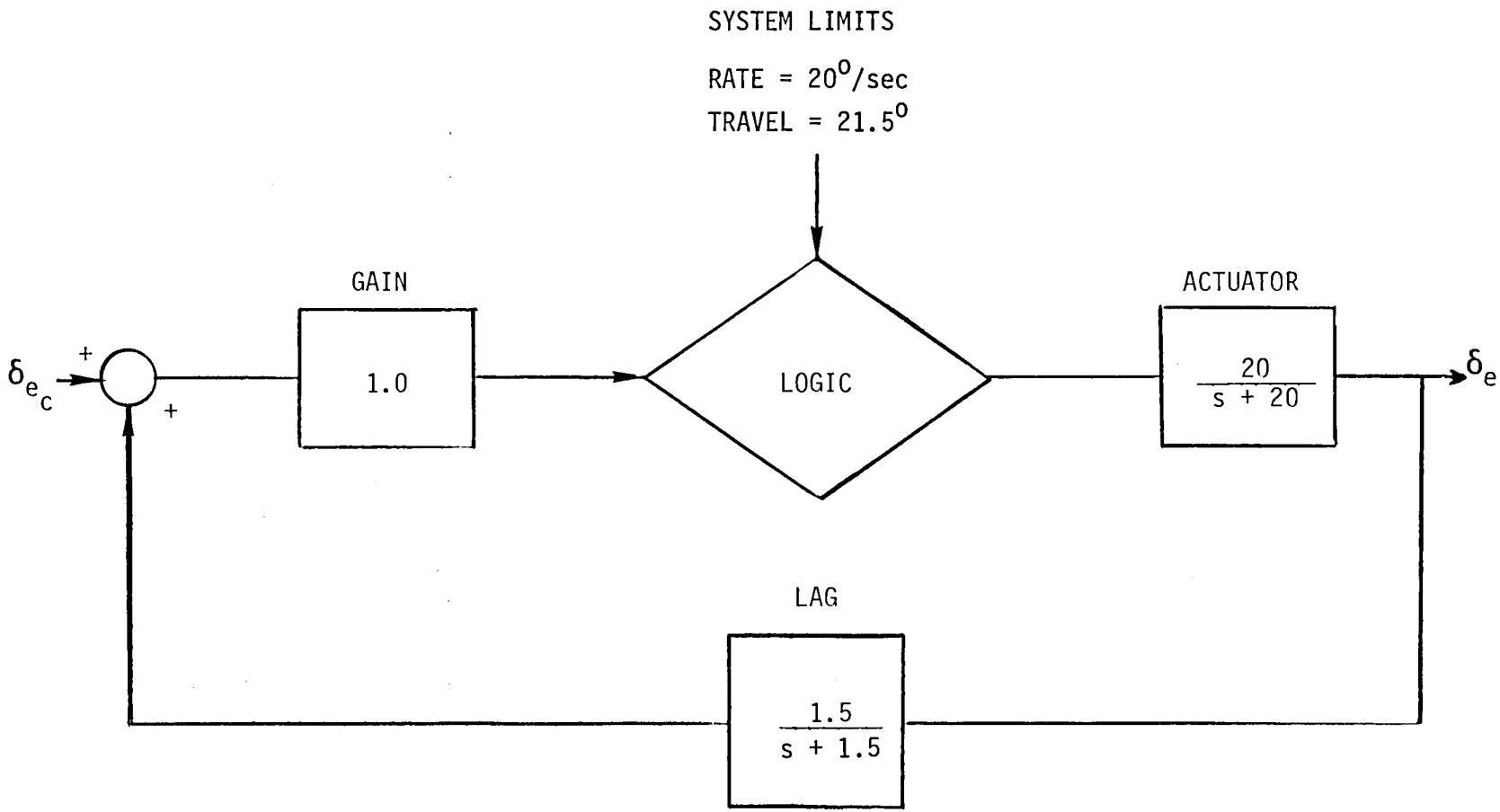

Figure 7. Simplified diagram of actuator loop used to obtain integration.

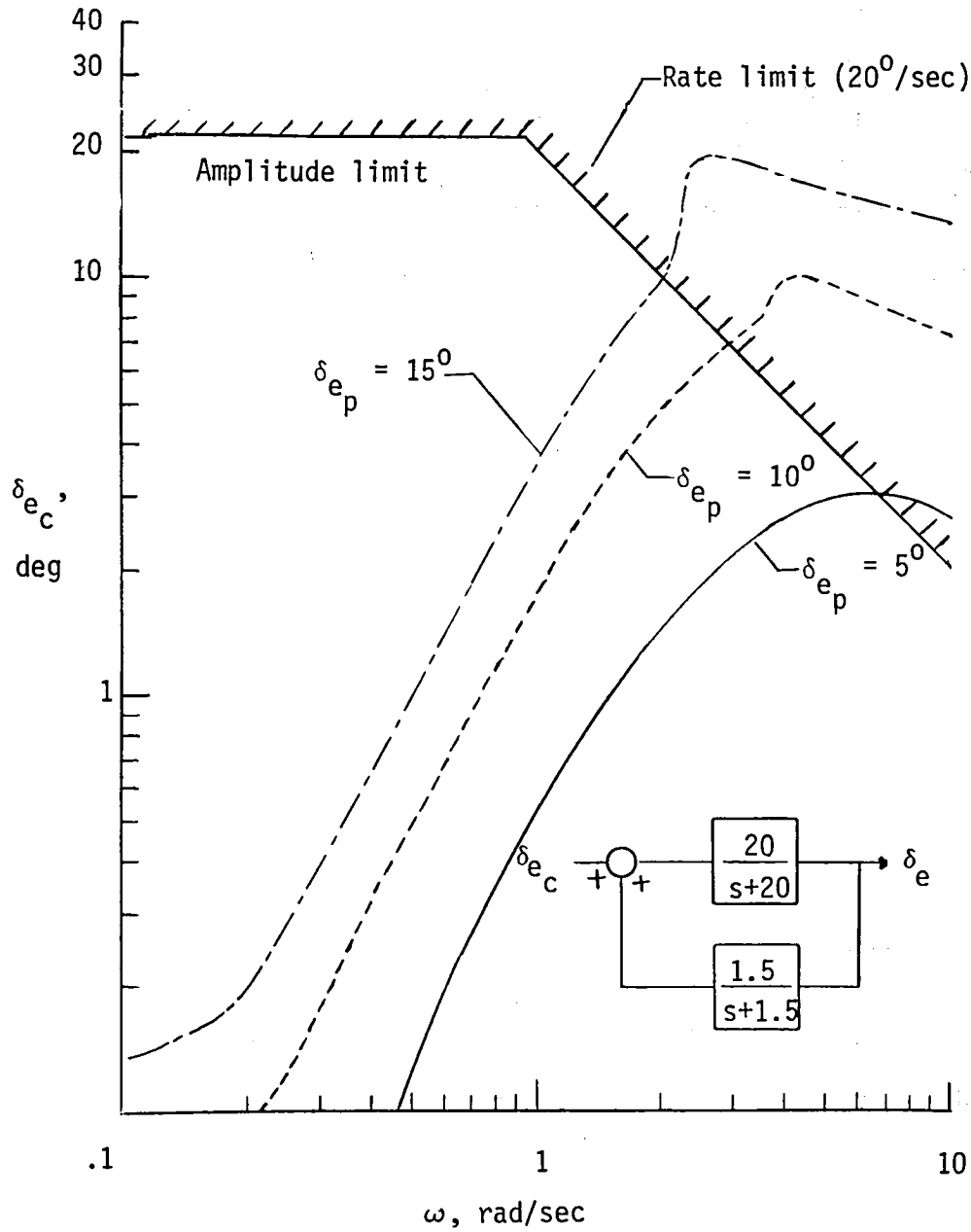

Figure 8. Commanded input to actuator loop as a function of pilot input and frequency.

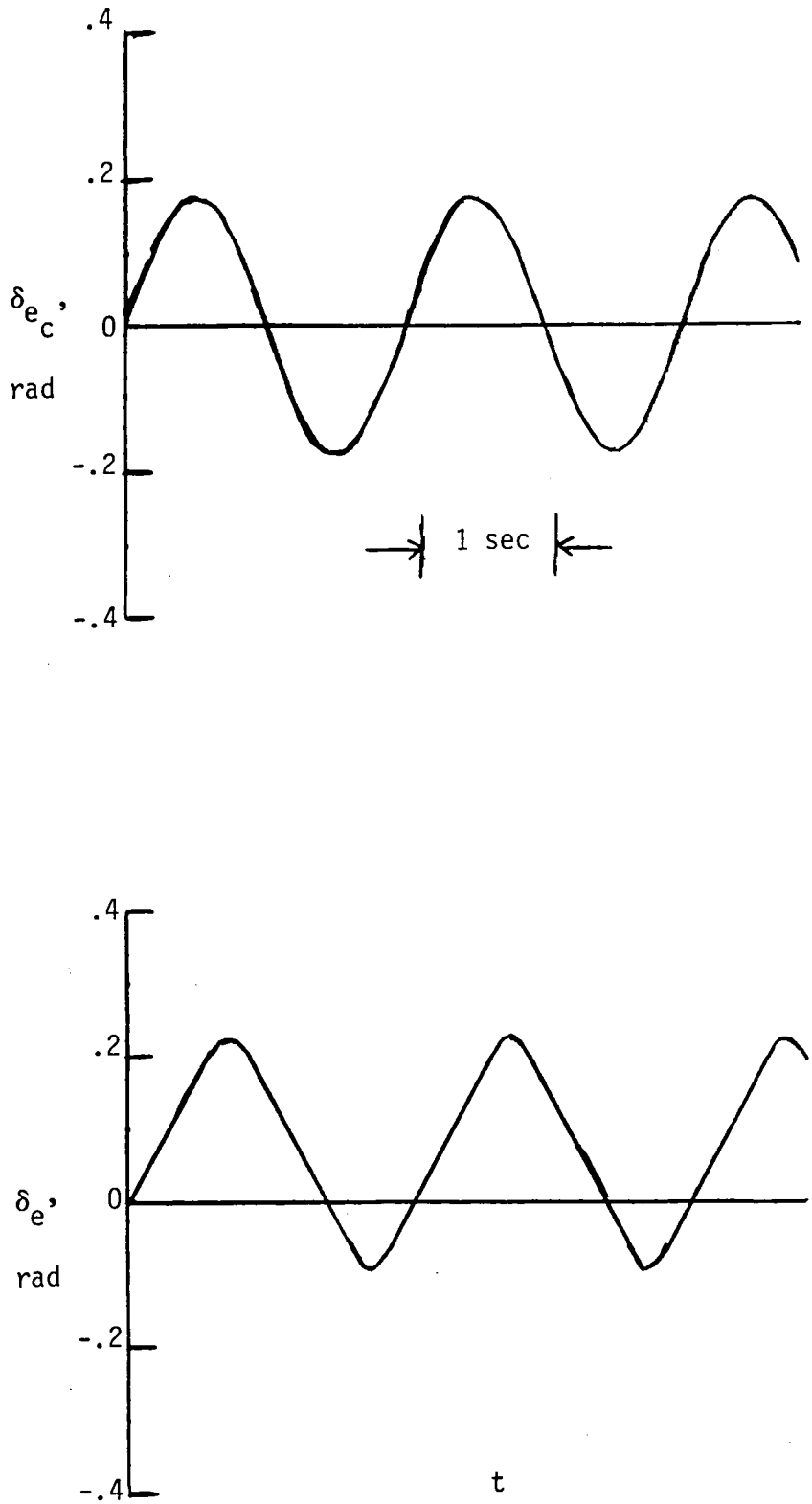

Figure 9. Digital simulation of actuator loop with a 20 degree per second rate limit. δ_{e_c} = A sin ωt; A = .174 rad or 10^o; ω = 3 rad/sec.

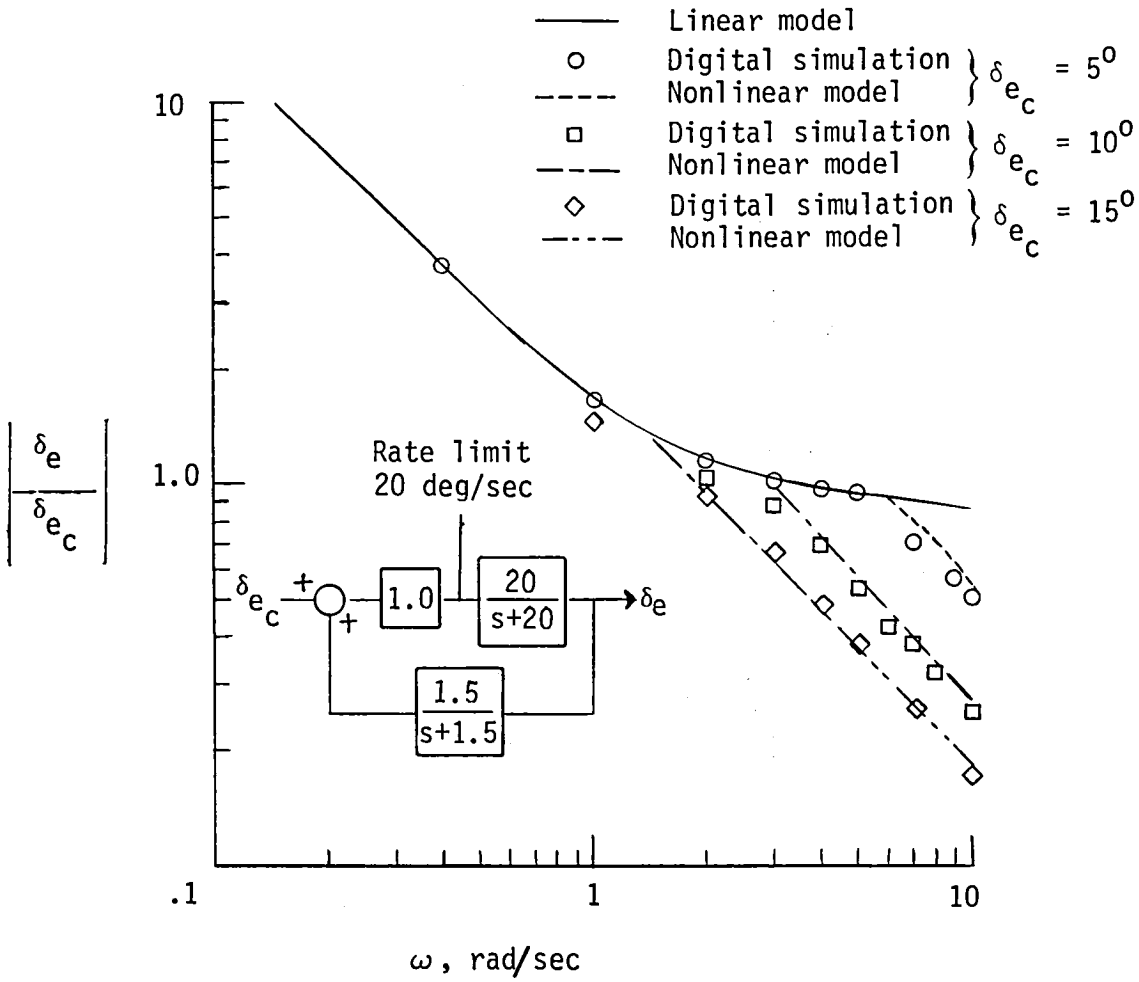

(a) Amplitude ratio.

Figure 10. Comparison of digital simulation with algorithm that describes actuator model.

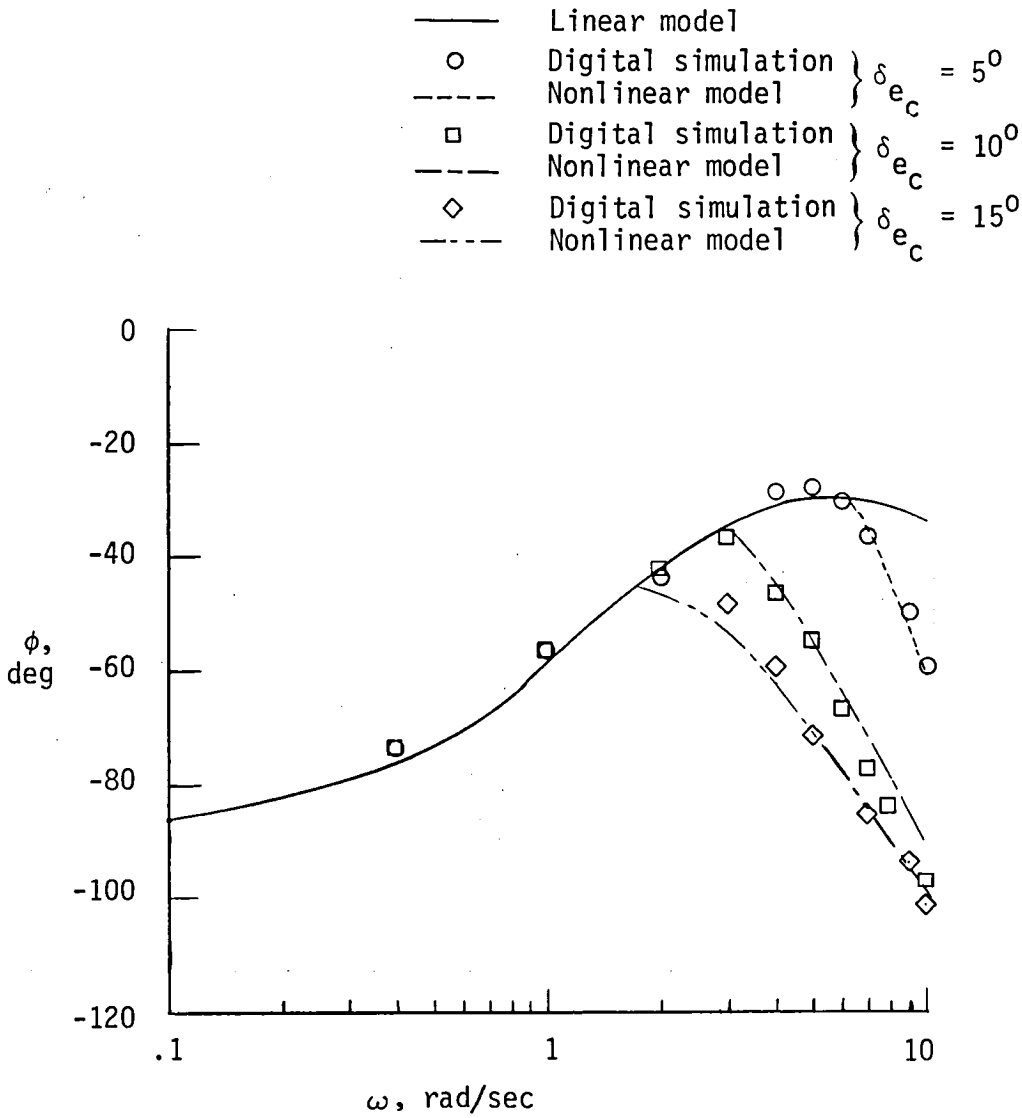

(b) Phase angle.

Figure 10. Concluded.

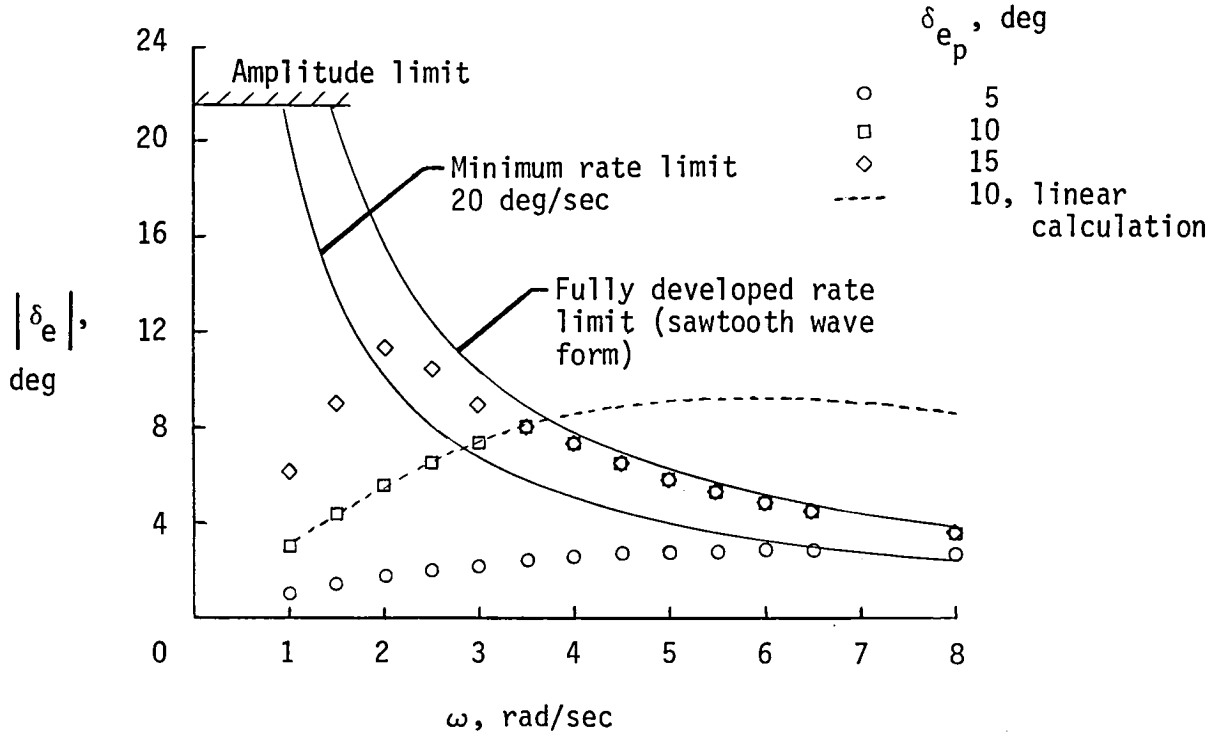

Figure 11. Elevon amplitude attenuation due to rate limiting as a function of frequency and pilot input. T = 0.1 second.

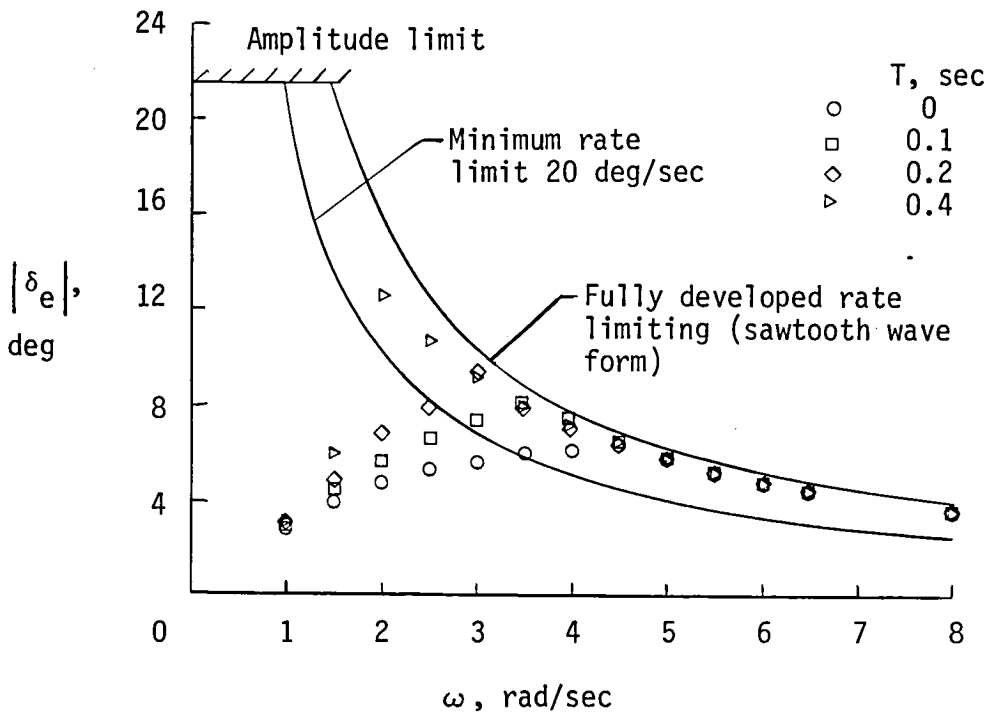

Figure 12. Elevon amplitude attenuation due to rate limiting as a function of frequency and time delay. $\delta_{e_p} = 10^o$.

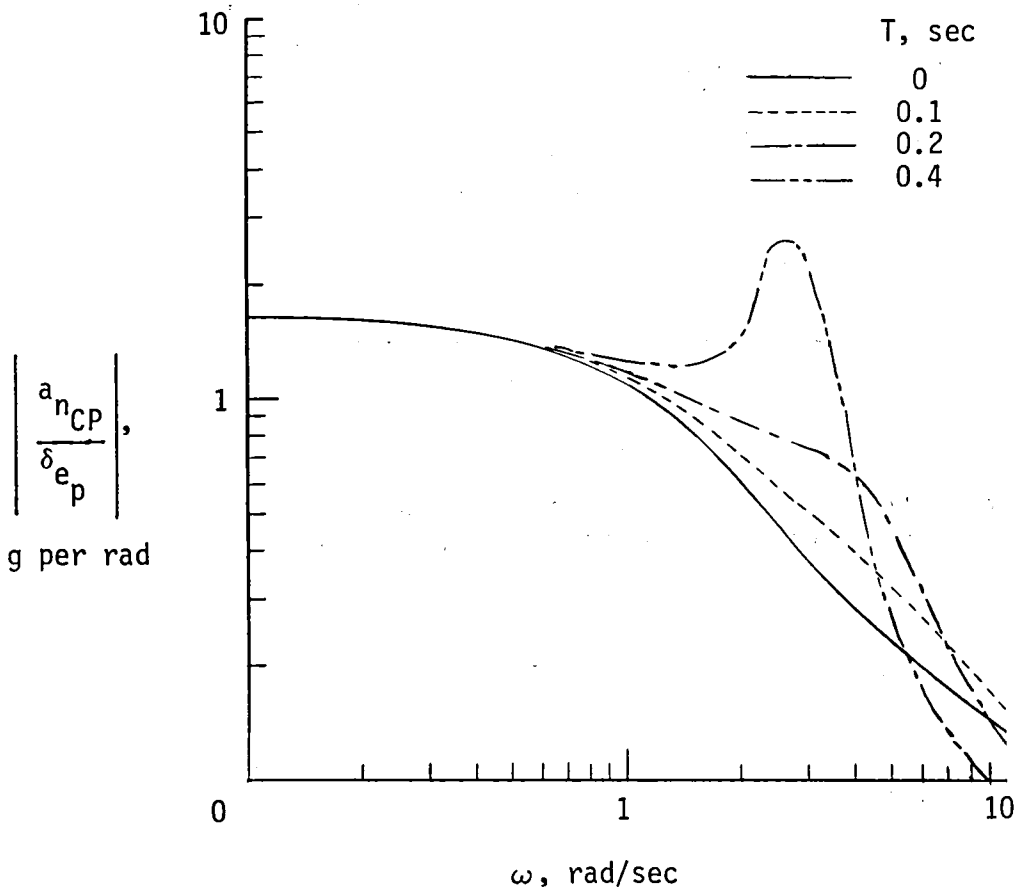

(a) Amplitude ratio.

Figure 13. Effect of time delay on normal acceleration at the cockpit. $\delta_{e_p} = 5^{o}$.

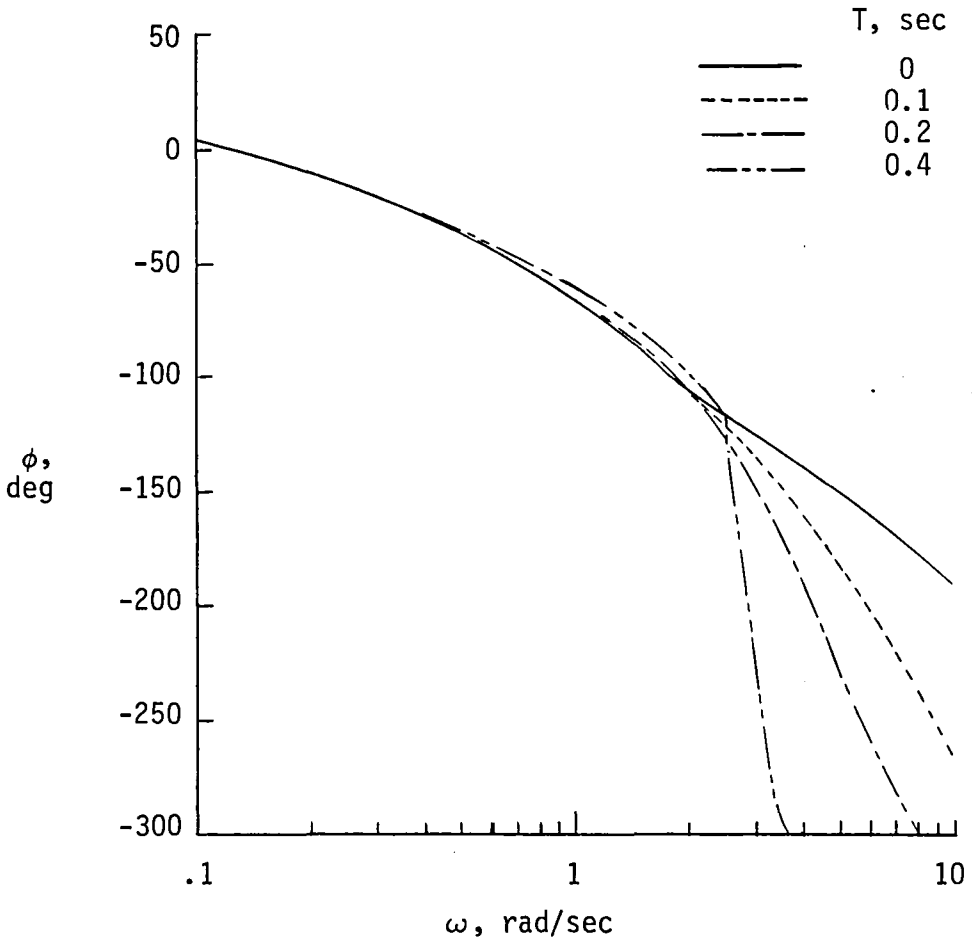

(b) Phase angle.

Figure 13. Concluded.

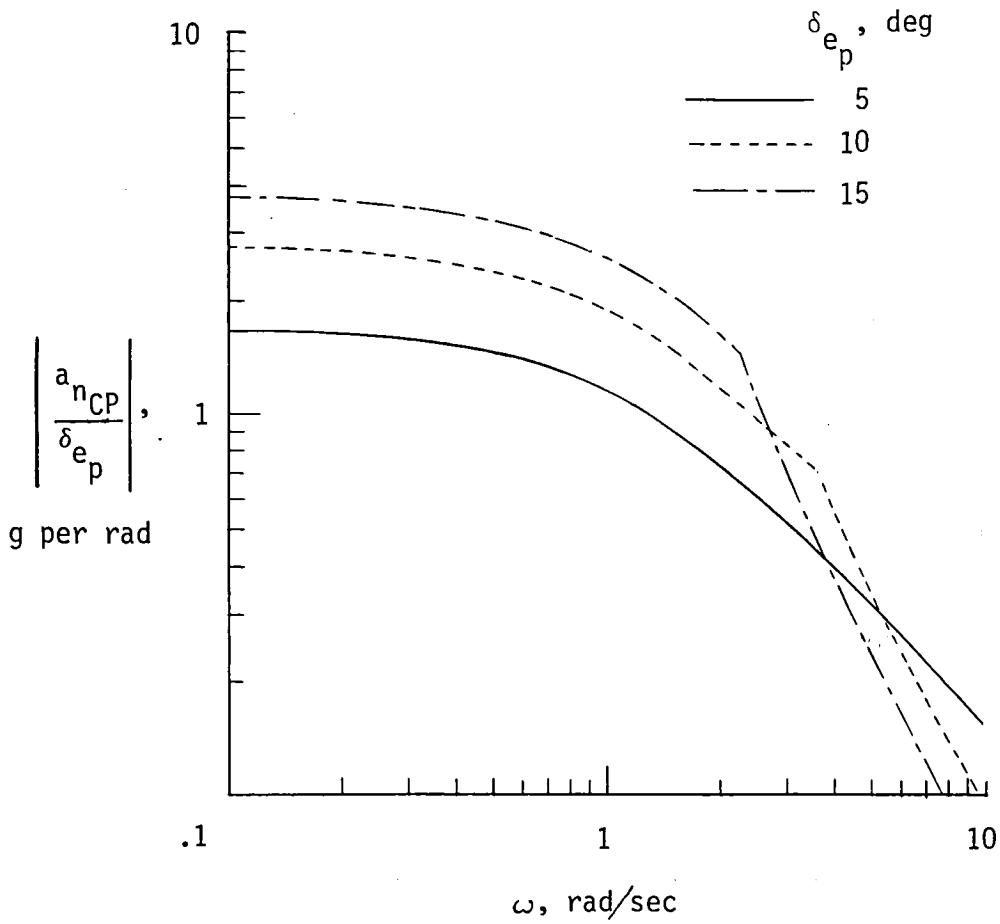

(a) Amplitude ratio.

Figure 14. Effect of pilot input on normal acceleration at the cockpit. T = 0.1 second.

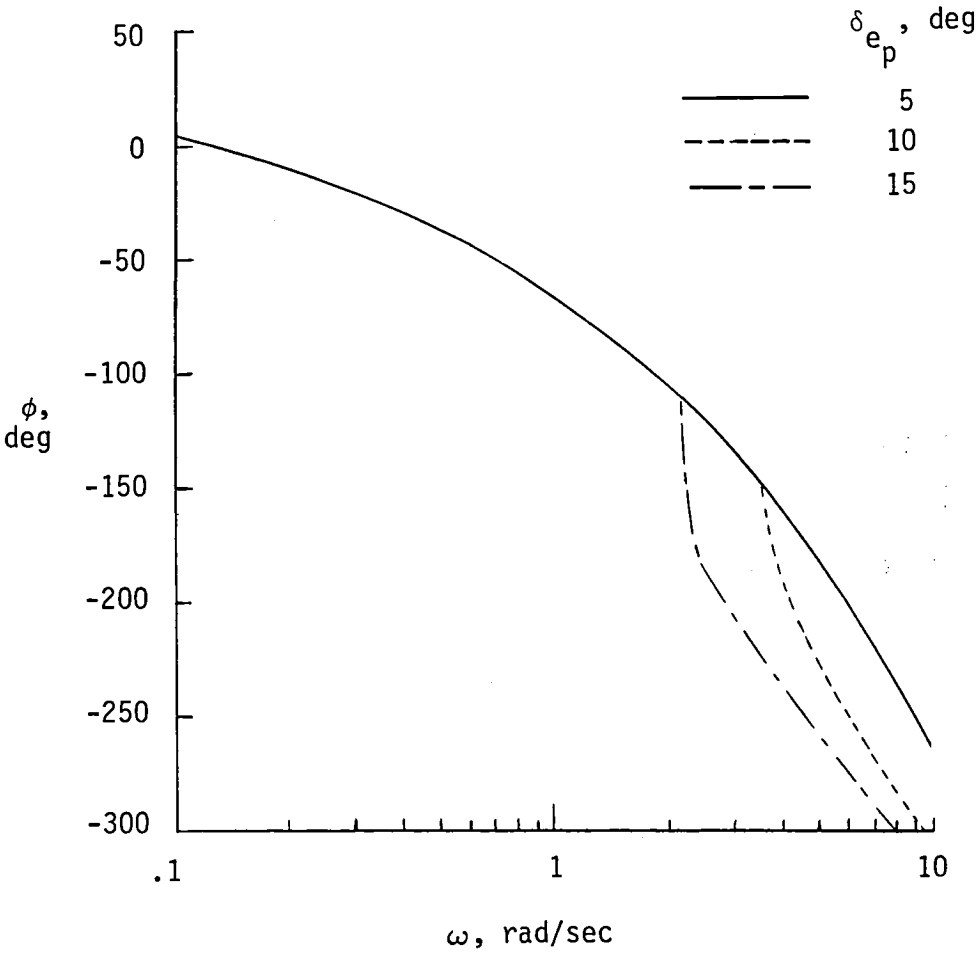

(b) Phase angle.

Figure 14. Concluded.

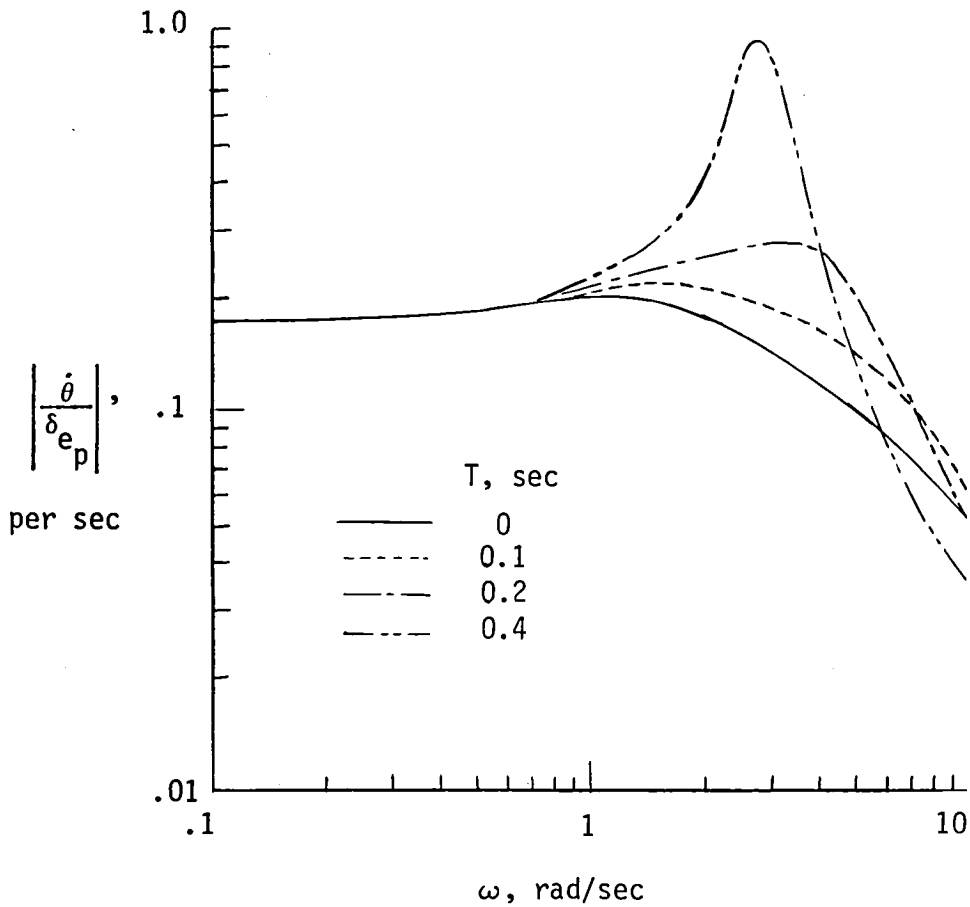

(a) Amplitude ratio.

Figure 15. Effect of time delay on pitch rate command system. $\delta_{e_p} = 5^o$.

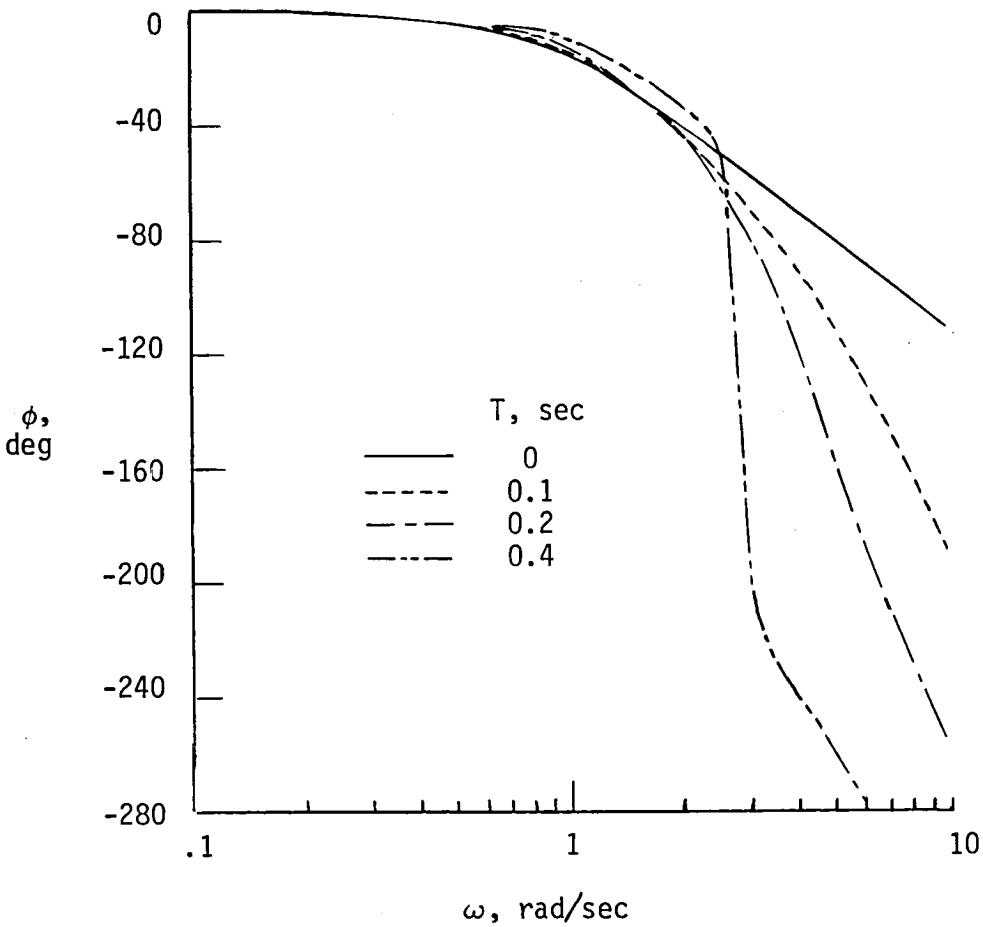

(b) Phase angle.

Figure 15. Concluded.

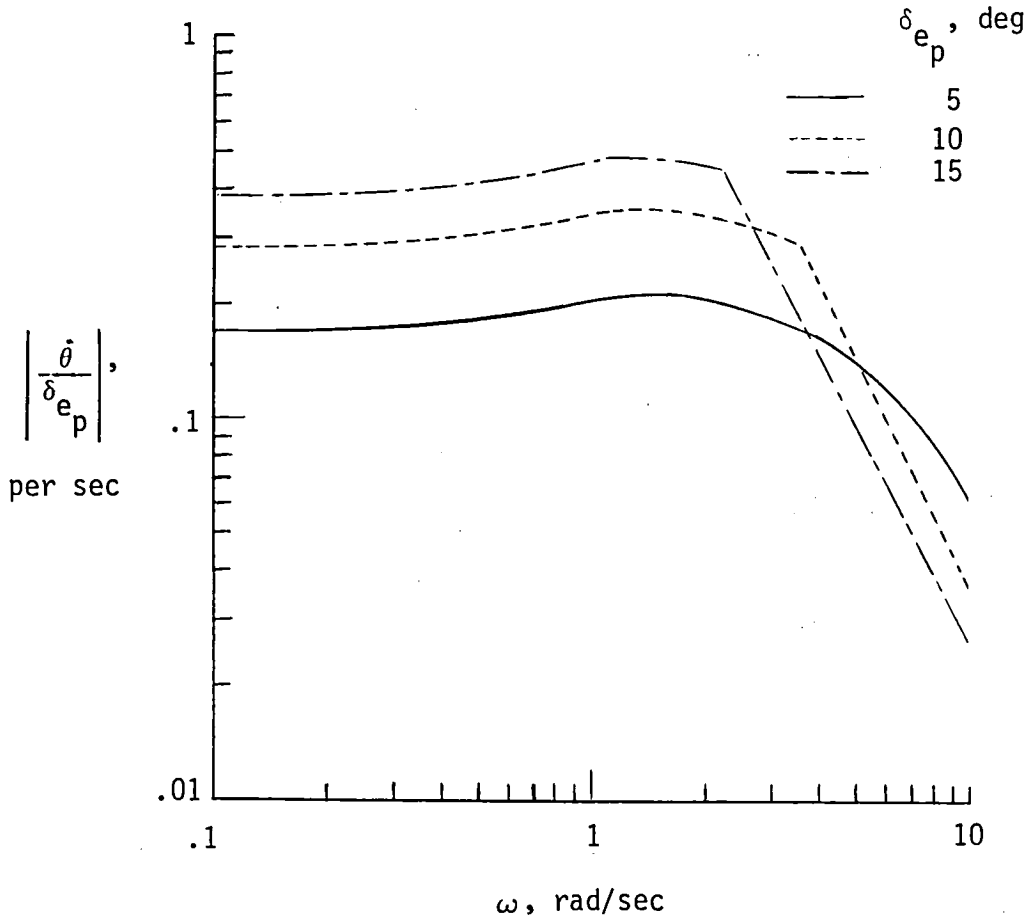

(a) Amplitude ratio.

Figure 16. Effect of pilot input on pitch rate command system. T = 0.1 second.

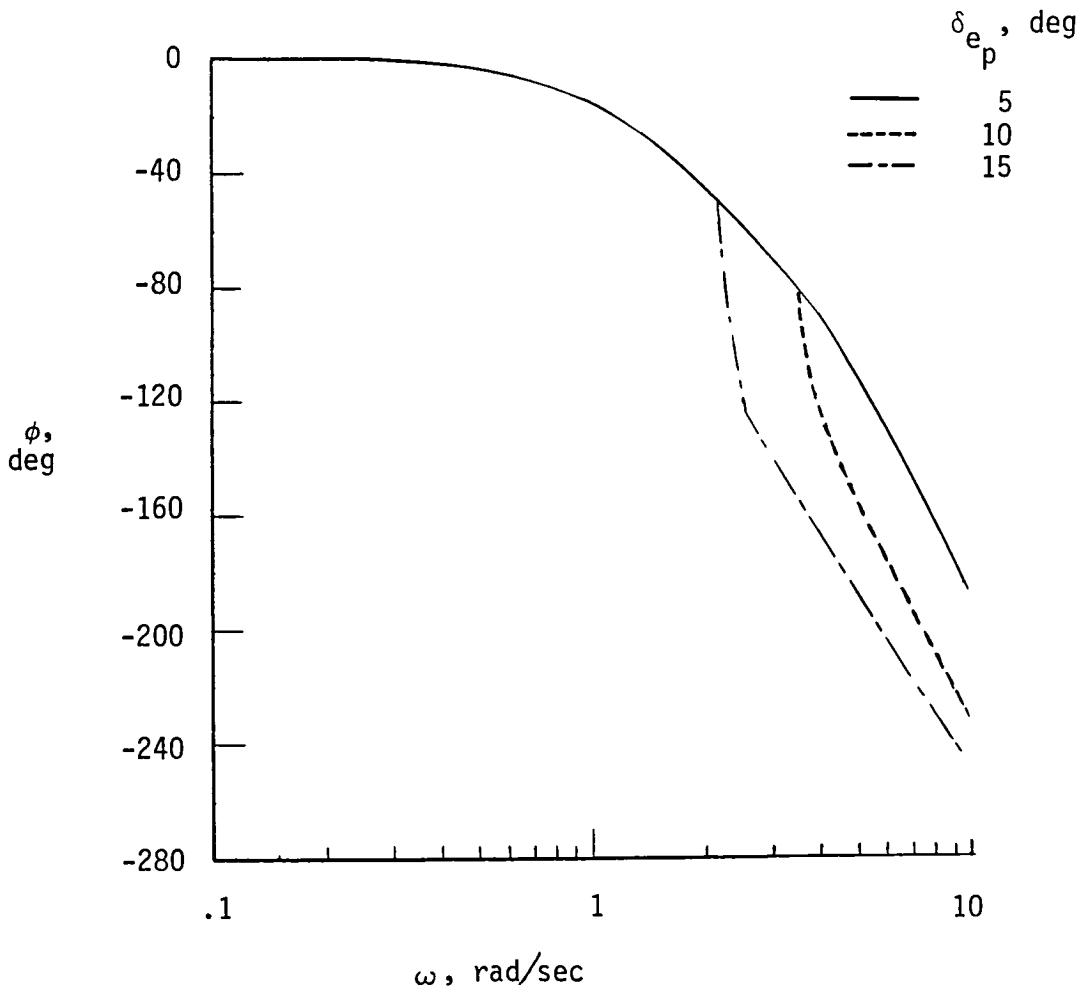

(b) Phase angle.

Figure 16. Concluded.

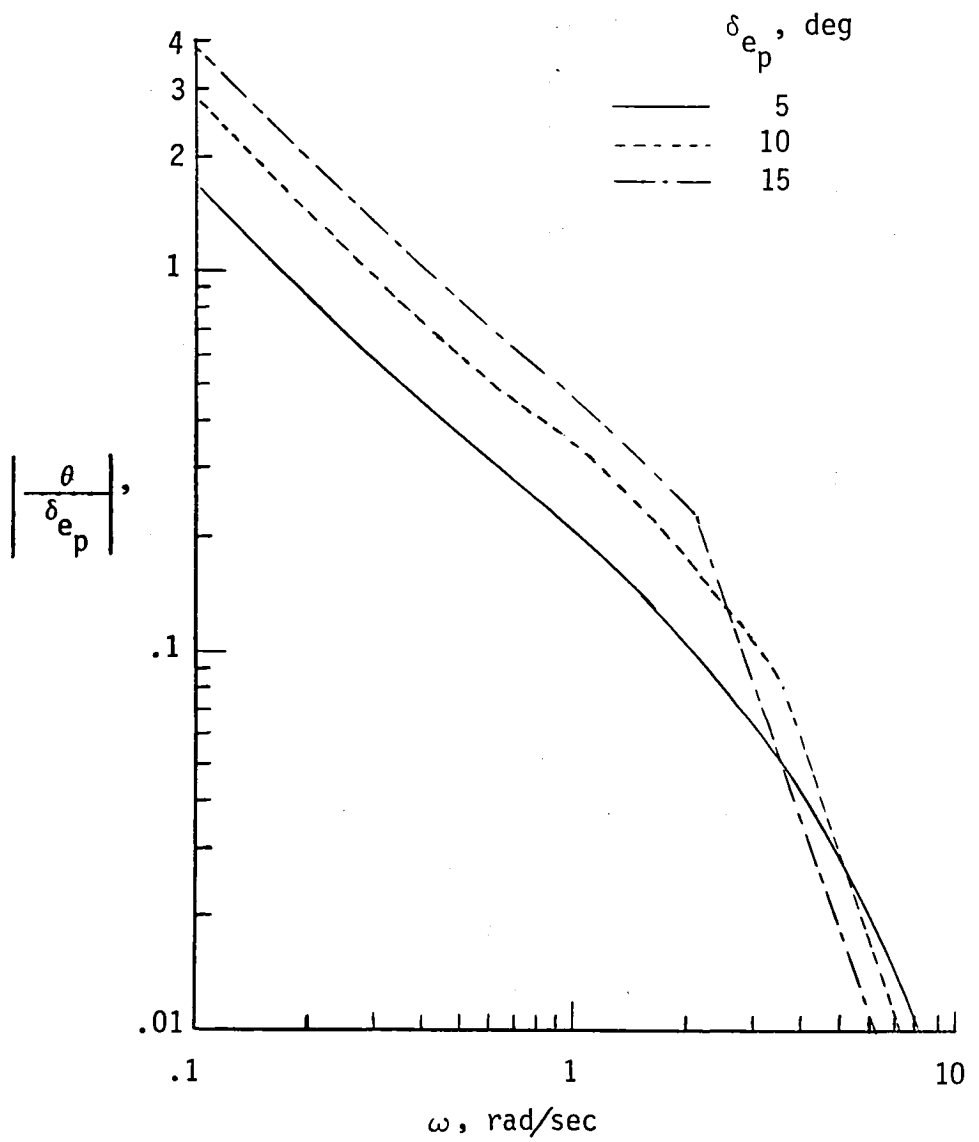

(a) Amplitude ratio.

Figure 17. Effect of pilot input on pitch attitude. T = 0.1 second.

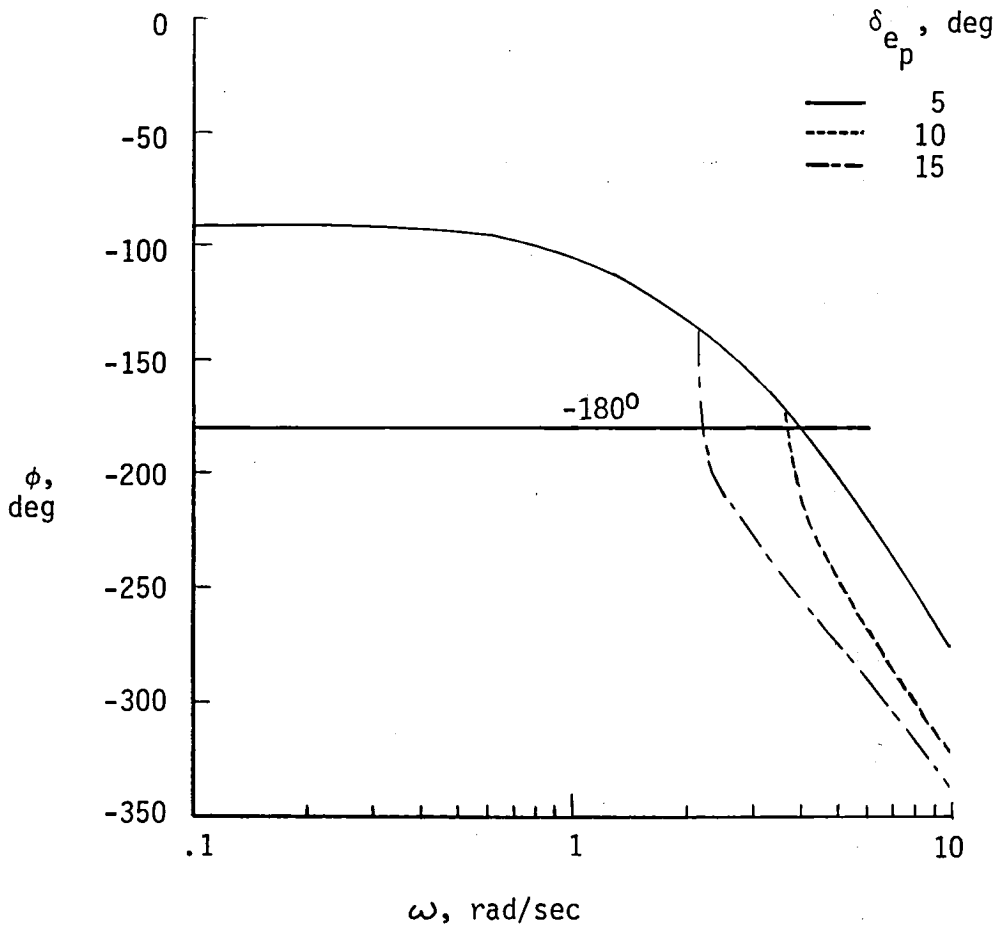

(b) Phase angle.

Figure 17. Concluded.

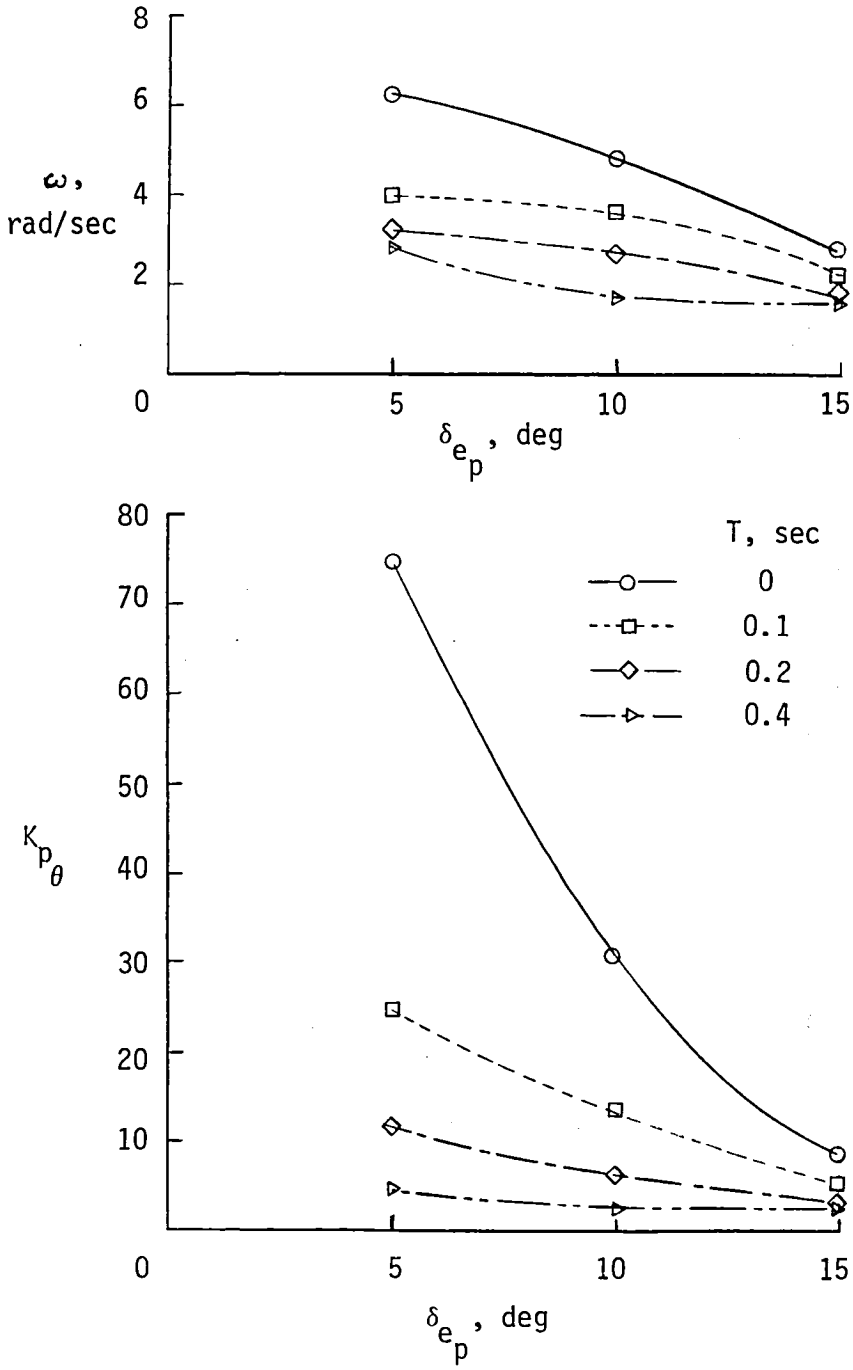

Figure 18. Frequency and minimum pilot gain required to PIO as a function of pilot input and time delay.

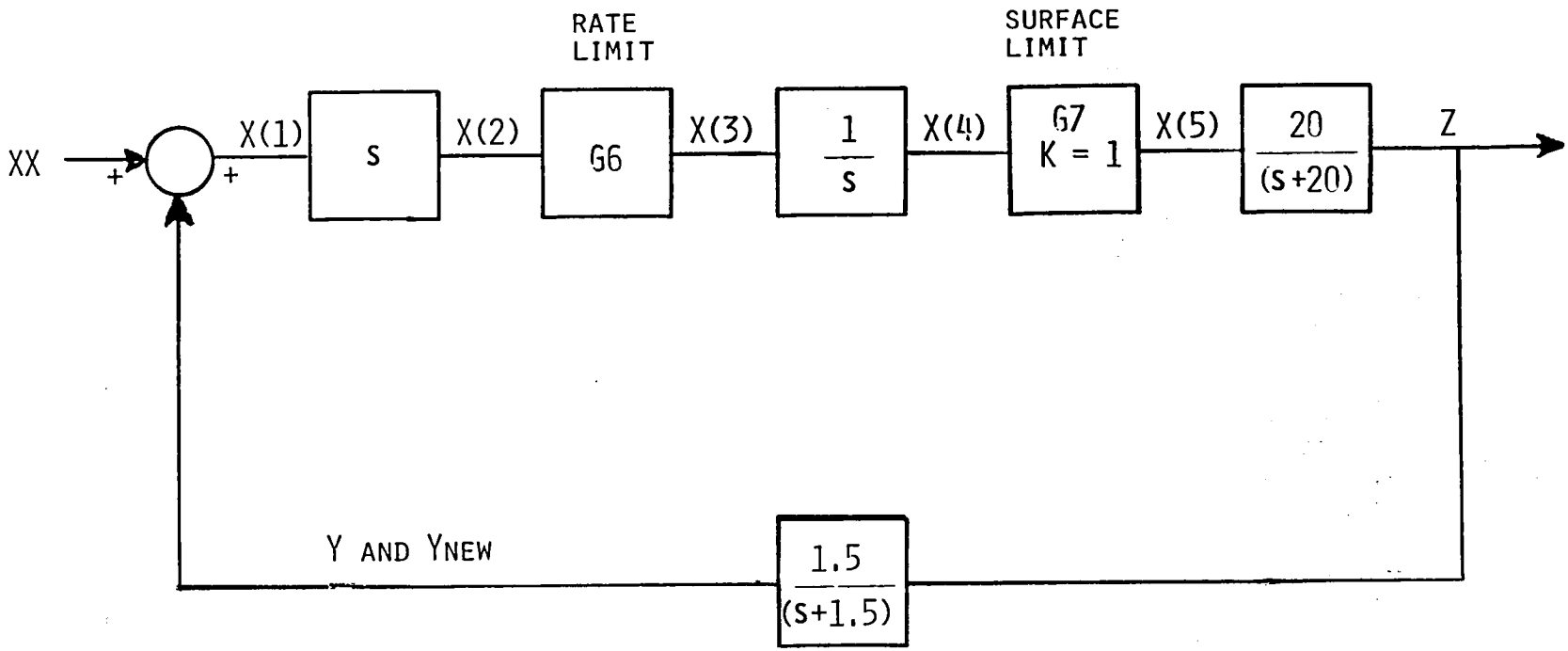

Figure 19. Actuator loop mathematical model.

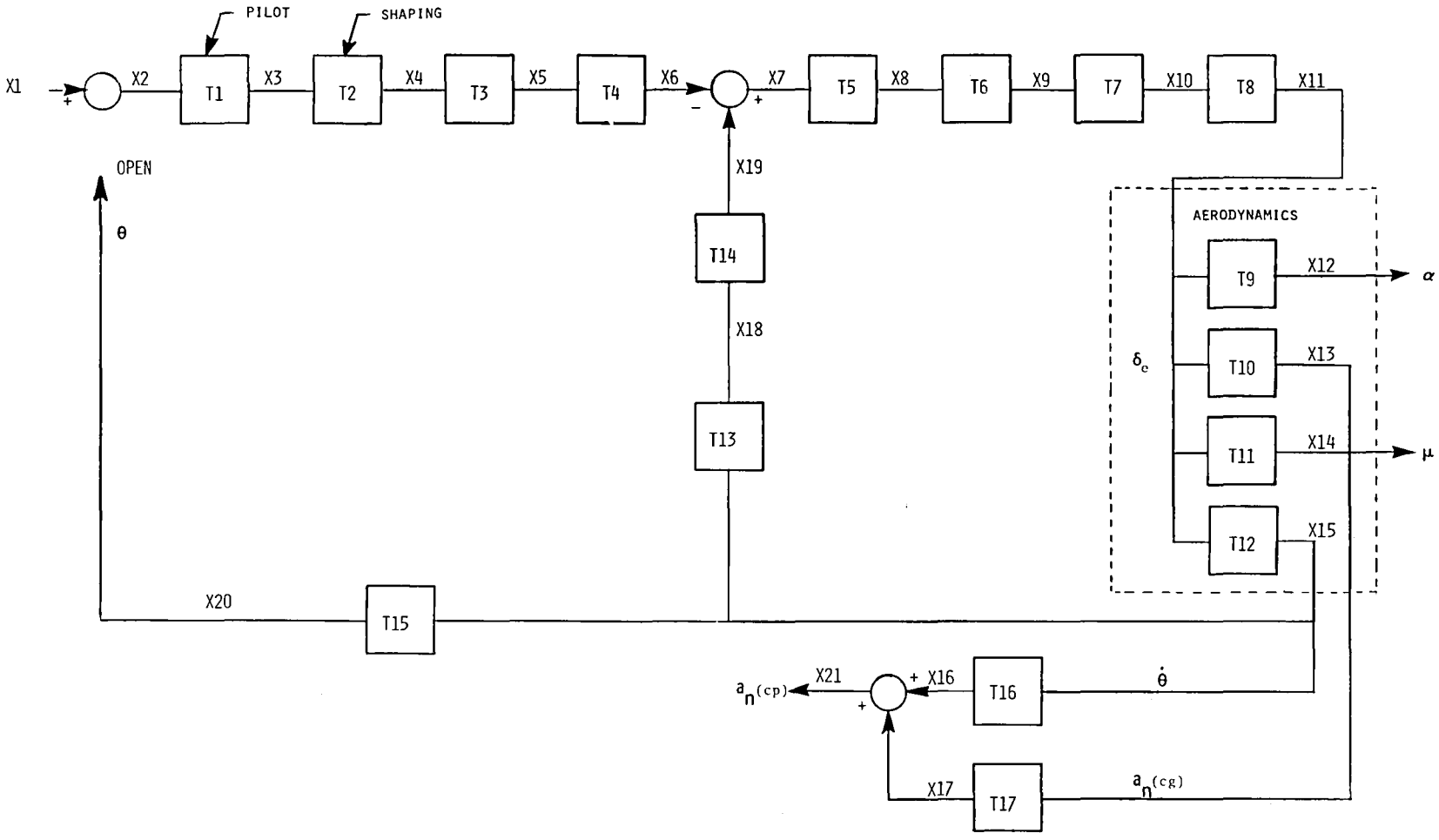

Figure 20. Shuttle mathematical model.

1. Report No.	2. Government Accession No.	3. Recipient's Catalog No.
NASA TM-81366		

4. Title and Subtitle	5. Report Date
ANALYSIS OF A LONGITUDINAL PILOT-INDUCED OSCILLATION EXPERIENCED ON THE APPROACH AND LANDING TEST OF THE SPACE SHUTTLE	December 1981
	6. Performing Organization Code: RTOP 505-43-14
7. Author(s): John W. Smith	8. Performing Organization Report No.
	10. Work Unit No.
9. Performing Organization Name and Address: Dryden Flight Research Facility, NASA Ames Research Center, P.O. Box 273, Edwards, California 93523	11. Contract or Grant No.
	13. Type of Report and Period Covered: Technical Memorandum
12. Sponsoring Agency Name and Address	14. Sponsoring Agency Code

15. Supplementary Notes

16. Abstract

During the final free flight (FF-5) of the shuttle's approach and landing tests, the vehicle experienced pilot-induced oscillations near touchdown. The flight test data showed that pilot inputs to the hand controller reached peak-to-peak amplitudes of 20° at a frequency between 3 and 3.5 radians per second. The controller inputs were sufficient to exceed the priority rate limit set in the pitch axis.

A nonlinear analytical study was conducted to investigate the combined effects of pilot input, rate limiting, and time delays. The frequency response of the total system is presented parametrically as a function of the three variables.

In general, with no dead time, for controller inputs of 5° or less, the total system behaves in a linear fashion. For 10° of controller input, independent of the delay time, the elevon loop will be rate saturated above a frequency of 4 radians per second.

17. Key Words (Suggested by Author(s))	18. Distribution Statement
Handling qualities Pilot-induced oscillations	Unclassified-Unlimited STAR category 08

19. Security Classif. (of this report)	20. Security Classif. (of this page)	21. No. of Pages	22. Price*
Unclassified	Unclassified	45	A03

For sale by the National Technical Information Service, Springfield, Virginia 22161